

Study of Negative and Positive Superhumps in ER Ursae Majoris

Tomohito OHSHIMA,^{1*} Taichi KATO,¹ Elena PAVLENKO,² Hidehiko AKAZAWA,³ Kazuyoshi IMAMURA,³
Kenji TANABE,³ Enrique de MIGUEL,^{4,5} William STEIN,⁶ Hiroshi ITOH,⁷ Franz-Josef HAMBSCH,^{6,8}
Pavol A. DUBOVSKY,⁹ Igor KUDZEJ,⁹ Thomas KRAJCI,¹⁰ Alex BAKLANOV,² Denis SAMSONOV,²
Oksana ANTONYUK,² Viktor MALANUSHENKO,² Maksim ANDREEV,¹¹ Ryo NOGUCHI,¹² Kazuyuki OGURA,¹²
Takashi NOMOTO,¹² Rikako ONO,¹² Shin'ichi NAKAGAWA,¹² Keisuke TANIUCHI,¹² Tomoya AOKI,¹²
Miho KAWABATA,¹² Hitoshi KIMURA,¹² Kazunari MASUMOTO,¹² Hiroshi KOBAYASHI,¹² Katsura MATSUMOTO,¹²
Kazuhiko SHIOKAWA,¹³ Sergey Yu. SHUGAROV,^{14,15} Natalia KATYSHEVA,¹⁴ Irina VOLOSHINA,¹⁴ Polina ZEMKO,¹⁴
Kiyoshi KASAI,¹³ Javier RUIZ,^{16,17} Hiroyuki MAEHARA,¹⁸ Natalia VIRNINA,¹⁹ Jani VIRTANEN,²⁰ Ian MILLER,²¹
Boyd BOITNOTT,⁶ Colin LITTLEFIELD,²² Nick JAMES,²³ Tamas TORDAI,²⁴ Fidrich ROBAERT,²⁴
Stefano PADOVAN,²⁵ Atsushi MIYASHITA,²⁶

¹ Department of Astronomy, Kyoto University, Kyoto 606-8502

* ohshima@kusastro.kyoto-u.ac.jp

² Crimean Astrophysical Observatory, 98409, Nauchny, Crimea, Ukraine

³ Department of Biosphere-Geosphere System Science, Faculty of Informatics, Okayama University of Science, 1-1 Ridai-cho, Okayama, Okayama 700-0005, Japan

⁴ Departamento de Física Aplicada, Facultad de Ciencias Experimentales, Universidad de Huelva, 21071 Huelva, Spain

⁵ Center for Backyard Astrophysics, Observatorio del CIECEM, Parque Dunar, Matalascañas, 21760 Almonte, Huelva, Spain

⁶ American Association of Variable Star Observers (AAVSO)

⁷ VSOLJ, 1001-105 Nishiterakata, Hachioji, Tokyo 192-0153

⁸ Vereniging Voor Sterrenkunde (VVS), Oude Bleken 12, 2400 Mol, Belgium

⁹ Vihorlat Observatory, Mierova 4, Humenne, Slovakia

¹⁰ Center for Backyard Astrophysics (New Mexico), PO Box 1351, Cloudcroft, NM 83117, USA

¹¹ Institute of Astronomy, Russian Academy of Sciences, 361605 Peak Terskol, Kabardino-Balkaria, Russia

¹² Osaka Kyoiku University, 4-698-1 Asahigaoka, Osaka 582-8582

¹³ Variable Star Observer's League in Japan (VSOLJ)

¹⁴ Sternberg Astronomical Institute, Lomonosov Moscow University, Universitetsky Ave., 13, Moscow 119992, Russia

¹⁵ Astronomical Institute of the Slovak Academy of Sciences, 05960, Tatranska Lomnica, the Slovak Republic

¹⁶ Observatorio de Cantabria, Ctra. de Rocamundo s/n, Valderredible, Cantabria, Spain

¹⁷ Agrupacion Astronomica Cantabra, Apartado 573, 39080-Santander, Spain.

¹⁸ Kiso Observatory, Institute of Astronomy, School of Science, The University of Tokyo, 10762-30 Mitake, Kiso-machi, Kiso-gun, Nagano 397-0101

¹⁹ Department of High and Applied Mathematics, Odessa National Maritime University, Ukraine

²⁰ Ollilantie 98, 84880 Ylivieska, Finland

²¹ Furzehill House, Ilston, Swansea, SA2 7LE, UK

²² Department of Physics, University of Notre Dame, Notre Dame, Indiana 46556, USA

²³ 1 Tavistock Road, Chelmsford, Essex CM1 6JL, UK

²⁴ Polaris Observatory, Hungarian Astronomical Association, Laborc utca 2/c, 1037 Budapest, Hungary

²⁵ American Association of Variable Star Observers, 49 Bay State Rd., Cambridge, MA 02138, USA

²⁶ Seikei Meteorological Observatory, Seikei High School, 3-3-1, Kichijoji-Kitamachi, Musashino-shi, Tokyo 180-8633

(Received 201 0; accepted 201 0)

Abstract

We carried out the photometric observations of the SU UMa-type dwarf nova ER UMa during 2011 and 2012, which showed the existence of persistent negative superhumps even during the superoutburst. We performed two-dimensional period analysis of its light curves by using a method called “least absolute shrinkage and selection operator” (Lasso) and “phase dispersion minimization” (PDM) analysis, and we found that the period of negative superhumps systematically changed between a superoutburst and the next superoutburst. The trend of the period change can be interpreted as reflecting the change of the disk radius. This change of the disk radius is in good agreement with the predicted change of the disk radius by the thermal-tidal instability (TTI) model. The normal outbursts within a supercycle showed a general trend that the rising rate to maximum becomes slower as the next superoutburst approaches. The change can be interpreted as the consequence of the increased gas-stream flow onto the inner region of the disk as the result of the tilted disk. Some of the superoutbursts were found to be triggered by a precursor normal outburst when the positive superhumps appeared to develop. The positive and negative superhumps co-

existed during the superoutburst. The positive superhumps were prominent only during four or five days after the supermaximum, while the signal of the negative superhumps became strong after the middle phase of the superoutburst plateau. A simple combination of the positive and negative superhumps was found to be insufficient in reproducing the complex profile variation. We were able to detect the developing phase of positive superhumps (stage A superhumps) for the first time in ER UMa-type dwarf novae. Using the period of stage A superhumps, we obtained a mass ratio of 0.100(15), which indicates that ER UMa is on the ordinary evolutionary track of cataclysmic variable stars.

Key words: accretion, accretion disks — stars: novae, cataclysmic variables — stars: dwarf novae — stars: individual (ER Ursae Majoris)

q

1. Introduction

Dwarf novae (DNe) are a class of cataclysmic variables (CVs), which consist of a white dwarf primary and a late-type secondary which fills its Roche lobe. The material transferred toward the primary through the inner Lagrangian point (L1) forms an accretion disk around the white-dwarf. The accretion disk causes instabilities, which are observed as an outburst [for reviews, see Warner (1995); Osaki (1996); Hellier (2001a)]. SU UMa-type stars are a subgroup of dwarf novae. They are characterized by the presence of two types of outbursts, normal outburst and superoutburst. Whereas a normal outburst lasts for only a few days, a superoutburst lasts for about two weeks and the maximum magnitude of the latter is brighter by 0.5–1 mag.

These objects also exhibit light variations called (positive) superhumps during superoutburst. The observed period of the superhumps is a few percent longer than the orbital period of the system. The positive superhumps are thought to arise by periodic viscous dissipation of tidally elongated disk (i.e. the eccentric disk) whose apsidal line slowly precesses in the prograde direction (see Whitehurst 1988, Hirose, Osaki 1990). On the other hand, some cataclysmic variables show variations shorter than the orbital period called “negative superhumps” (Udalski 1988; Harvey et al. 1995; Ringwald et al. 2012). The origin of negative superhumps is usually considered as a result of retrograde precession in a tilted accretion disk (Wood, Burke 2007). When the disk is tilted, the hot spot is formed at the inner part of the disk, not the edge of the disk. Since the energy of hot spot comes from the release of gravitational energy, such change in the location of the hot spot causes a variation in the amount of the released energy, namely the luminosity of the hot spot. Combined with the retrograde precession, this effect can explain the negative superhumps.

The interval of successive two superoutbursts is called “supercycle”. These two superoutbursts usually sandwich several normal outbursts. In order to explain such behavior of SU UMa-type dwarf novae, the tidal thermal instability (TTI) model is suggested (Osaki 1989). In this model, systems with small mass ratios ($M_2/M_1 = q \leq 0.25$) enable the disk to reach the radius of the 3:1 resonance to the orbital motion of the secondary. In normal outbursts, the material of the disk only partly accrete to the inner region. The radius of the disk becomes gradually larger after experiencing normal outburst. When the disk radius reaches the 3:1 resonance radius, the eccentric instability is excited. The increased turbulence in the disk causes an increase in the mass-transfer rate in the disk and a long, bright superoutburst is triggered (Osaki 1989). This prograde precession also causes the superhump (Whitehurst 1988, Hirose, Osaki 1990).

ER UMa is a member of SU UMa-type dwarf novae and its intervals of superoutburst (supercycle) are as short as 40 – 50 d (Kato, Kunjaya 1995). This object is known as the prototype of a subgroup, “ER UMa type” which is characterized by having extremely short supercycles (< 60 d) among SU UMa-type stars (e.g. Robertson et al. 1995, Nogami et al. 1995; for a review see Kato et al. 1999). Although Gao et al. (1999) and Kjurkchieva, Marchev (2010) suggested on the presence of negative superhumps during quiescence and a normal outburst, only positive superhumps were observed during the following superoutburst. However, Ohshima et al. (2012) reported that negative superhumps were detected in ER UMa during the superoutburst in 2011 January. This is the first confident detection of negative superhumps during the superoutburst of any SU UMa-type dwarf nova. In Ohshima et al. (2012) (hereafter paper I), we reported the persistent negative superhump was detected in ER UMa and implied the possibility that the existence of negative superhumps suppresses of the occurrence of normal outbursts.

The existence of negative superhumps during superoutburst was also reported in other SU UMa-type dwarf novae V1504 Cyg and V344 Lyr (Osaki, Kato 2013a, Still et al. 2010). Osaki, Kato (2013a) analyzed data of an SU UMa-type dwarf nova V1504 Cyg observed by Kepler, and showed that this object also shows negative superhumps during superoutburst as well as during normal outbursts and in quiescence. Osaki, Kato (2013a) have demonstrated that in V1504 Cyg the frequency of occurrence of normal outbursts in a supercycle is related to the existence or non-existence of negative superhumps in the sense that it is reduced when the negative superhumps exist, confirming the suggestion made in Paper I. That is, the cycle lengths of normal outbursts are longer in a supercycle with negative superhumps than those in a supercycle without negative superhumps, and they called the former case “type L-supercycle” and the

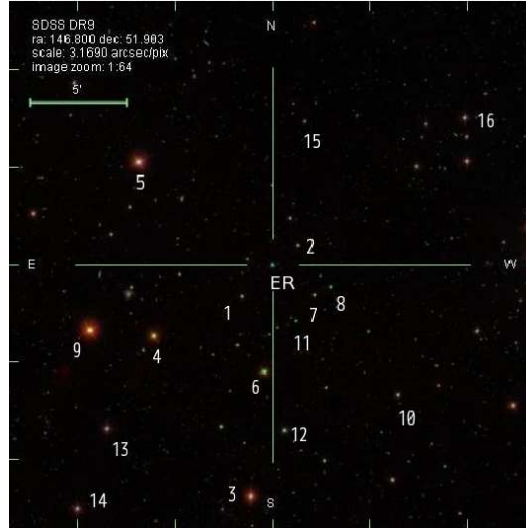


Fig. 1. Finding chart of ER UMa and the comparison stars. (derived from <http://cas.sdss.org/dr7/en/tools/chart/chart.asp>)

latter case “type S-supercycle” (these two types were first introduced by Smak (1985) for supercycles observed in VW Hyi and symbols “L” and “S” come from “long” and “short” for normal outburst cycles).

In Paper I, we dealt with only one supercycle of ER UMa in 2011. We have made further comprehensive observations of ER UMa in 2011 and 2012 and, our dat covered three supercycles in 2011 and three supercycles in 2012. All of supercycles observed have turned out to be were all accompanied with negative superhumps, and provide an excellent opportunity to study the outburst behavior when negative and positive superhumps co-exist. In this paper, we report on these new observations together with a more sophisticated analysis of the data reported in paper I. We explain our observations in section 2 and we present the result of their analysis observation and analysis in section 3. The conclusion is given in section 4.

2. Observations

We performed time-resolved photometric observations of ER UMa at 21 observatories scattered world-wide from 2011 January to 2012 December as a part of the VSNET Collaboration (Kato et al. 2004). We could obtain data of 146 nights in 2011, and 161 nights in 2012. The log of observatories is given in table 1, where (1) the first column is the abbreviation of observer, (2) names of observer or observatory, (3) instrument used, and (4) comparison stars used. The journal of observations is summarized in table 4 (given Appendix in the Electric version). The chart of ER UMa and its comparison stars is presented in figure 1.

After dark-subtracting and flat-fielding in CCD observations, we performed aperture photometry of the variable and its comparison stars and obtained differential magnitudes. All observed times were transformed to barycentric Julian Days (BJD). We made corrections for the systematic differences between observers after that.

3. Result

In this section, we first present the results of our observations and their analysis then discuss their implications. We describe first the outburst behaviors of ER UMa in subsection 3.1, and we then discuss the negative superhumps and the positive superhumps in subsection 3.2, and 3.3, respectively, and we finally deal with the transition from negative superhump to positive superhump in subsection 3.4.

3.1. Outburst Light Curves

3.1.1. The overall light curves of ER UMa in 2011 and 2012

The overall light curve of ER UMa is presented in figures 2 for 2011 and 3 for 2012. The entire list of observed superoutbursts is shown in table 2, where (1) the first column is the identification of the superoutburst, (2) its starting date in BJD, (3) The date of BJD of the supermaximum, and (4) the length of supercycle, where the supercycle is defined from the starting date of the previous superoutburst to that of the current one. As seen in the figure 2 and 3, three superoutbursts in 2011 (2011 S1-S3) and three superoutbursts in 2012 (2012 S1-S3) were clearly observed during this observational campaign although a possible superoutburst candidate was also observed in 2012 (2012 S4) but it was unclear because of sparse data points. The length of observed of supercycles were in a range of 44–58 d. These

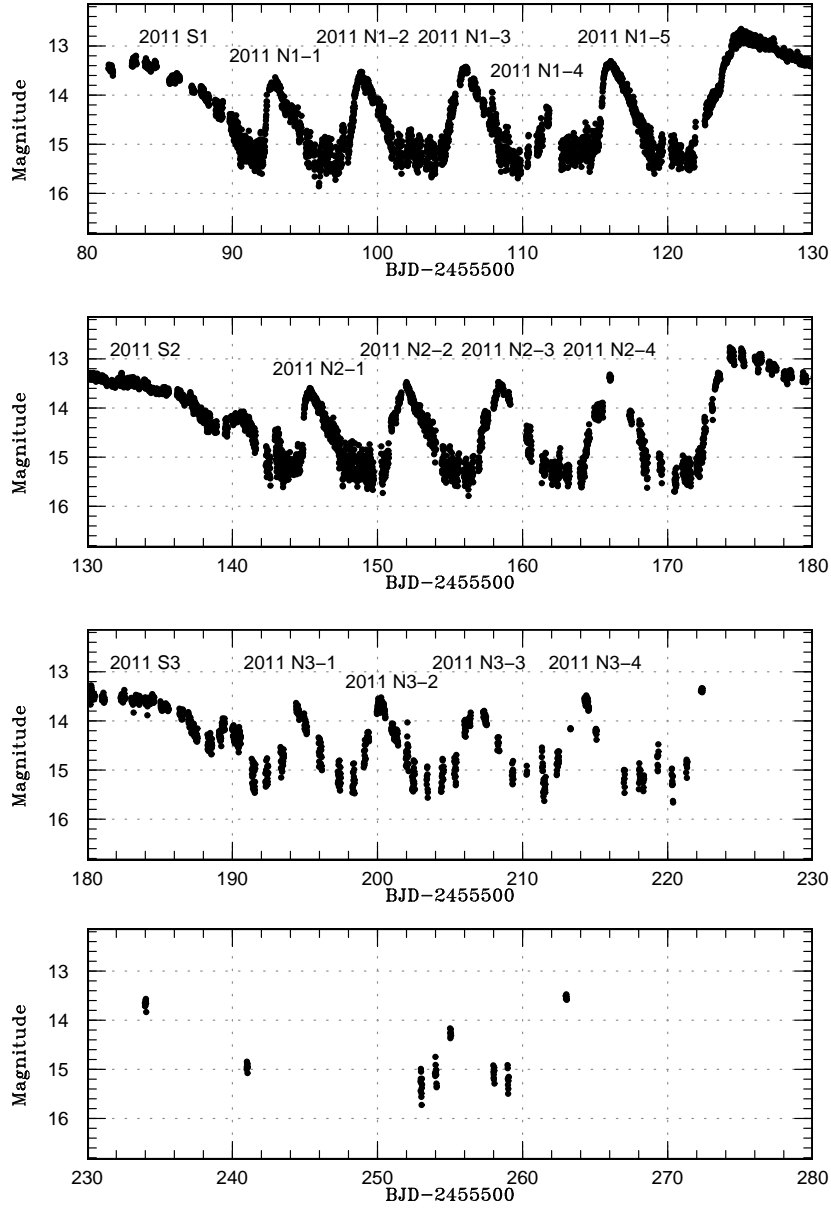


Fig. 2. Entire light curve of ER UMa of the 2011 season. The observed data is binned to 0.01 d.

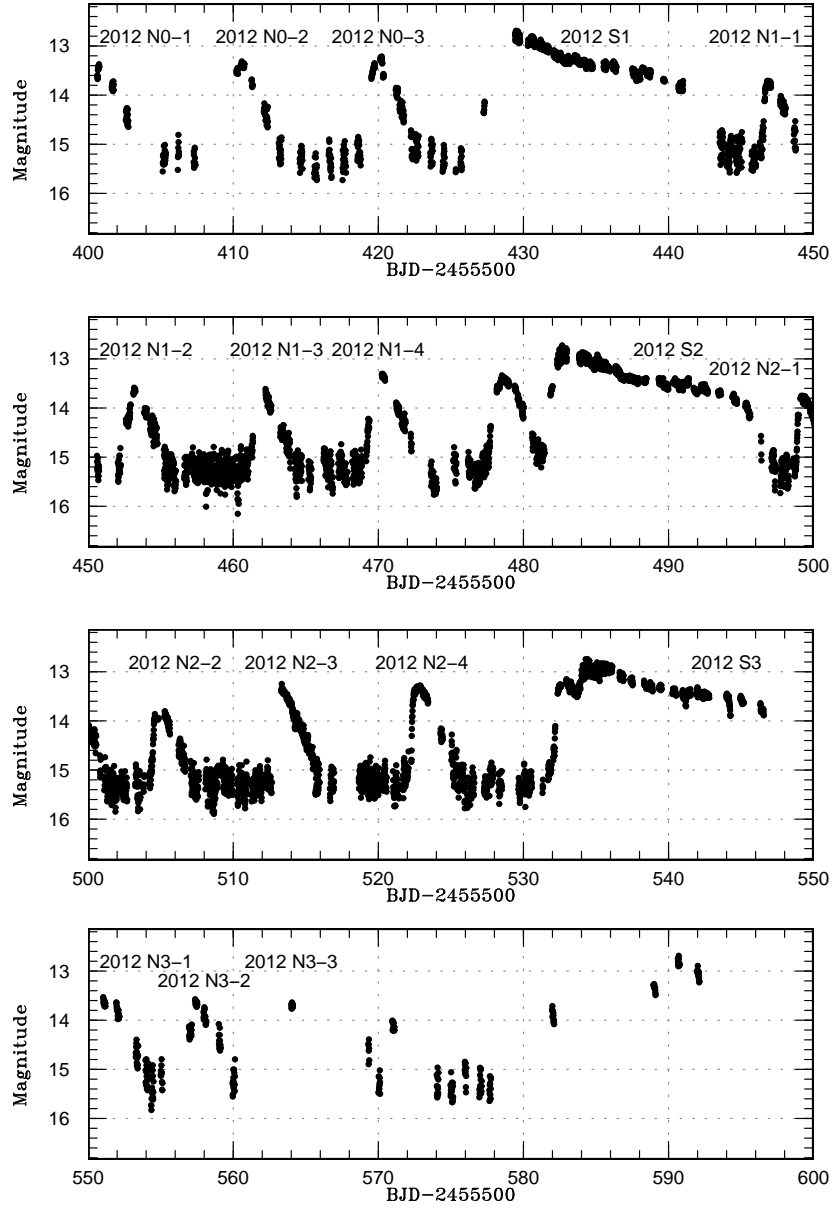


Fig. 3. Entire light curve of ER UMa of the 2012 season. The observed data is binned to 0.01 d.

Table 1. Log of observatories

The key to Observer	Observer or Observatory Name	Instrument	Comp
KU	Kyoto University	40cmSCT+ST-9E	1
Aka	Akazawa Hidehiko	28cmSC,35.5cmSC + ST-7XE, ST-9XE	1,4,5
AKz	Astrokolkhoz team*	30cmSC+ST-9,35cmSC+ST-8	2
APO	Apache Point Observatory	50cmC+SITe	6
BBo	Boyd Boitnott	28cmSC+QSI-516wsg	6
CRI	Crimean Astroph. Obs.	60cm+Apogee Alta E47	6
deM	Enrique de Miguel	28cmSC+QSI-516wsg / 25cmL	2
DPV	Pavol A. Dubovsky	28cmL+DSI ProII	6
Ham	Frantz-Josch Hambsch	40cm+STL11	2
Ioh	Itoh Hiroshi	30cmSC+DSI-Pro	6
IMi	Ian Miller	35cmSC+SXVR-H16	1,2,11
Kai	Kasai Kiyoshi	28cmSC+ST-7XME	1,4
Kra	Tom Krajci	28cmSC+SBIG ST-8	6
LCO	Colin Littlefield	28cmSC+ST-8XME	5,13,14
Mhh	Hiroyuki Maehara	25cmL+ST-7XME	4
NDJ	Nick James	28cmSC+SBIG ST-9XE	2
NKa	Natalia Katysheva	50cmR, 14cmC+ST-10XME	1,2,4,6, 8,9,10,12
OKU	Osaka Kyoiku Univ.	51cm+ST-10	1
OUS	Okayama Univ. of Sci. team	23.5cmSC+ST-8	6
PSD	Stefano Padovan	25cm epsilon+ST-10XME	1,3,8, 10,13,15
Pol	Polaris Observatory	ST-7E	4
Rui	Jevier Ruiz	0.4mRC+ST-8XME	1
Sac	Seikei High School	15.2cmR+ST-9E	5
Shu	Sergey Shugarov	50cmR, 14cmC+ST-10XME	1,2,4,6, 8,9,10,12
Siz	Siokawa Kazuhiko	35SC+ST-9E	4
SAO	Special Astrophysical Observatory [†]	1m+EEV CCD42-40'	1,2,4,6, 8,9,10,12
SWI	William Stein	C14+SBIG ST-10XME	2
Ter	Terskol Observatory	C14+STL1001	6
Vir	Jani Virtanen	C14+SBIG ST-10XME	6
VIR	Natalia Virnina	60cm	6
Vol	Irina Voloshina	60cmL+Apogee 47	11

1: GSC 3439.629, 2: GSC3439.920 3: GSC3439.1287 4: TYC2-3439.1099.1 5: TYC3439.1253.1

6: GSC3439.669 7: GSC3439.816 8: GSC3439.957

9: GSC3439.1211 10: GSC3439.745 11: USNO1350.07816004

12: GSC3439.1105 13: GSC3439.911 14: TYC2-3439.916.1

15:GSC3439.1091 16: GSC3439.885

*by F. J. Hambsch and T. Krajci

[†]by Natalia Katysheva

values are in agreement with the previous report (Zemko et al. 2013). Table 3 shows the list of normal outbursts. The first column is the identification of a normal outburst. Here 2012 N2-3, for instance, indicates the third normal outburst in supercycle No.2 in 2012. We see from table 3 that the maximum magnitude of normal outburst gets brighter and the length of normal outburst cycles gets longer as the object approaches the next superoutburst (i.e. with an advance of supercycle phase), although there exists some exceptions (e.g. the interval between 2012 N1-2 and 2012 N1-3 is longer than that between 2012 N1-3 and 2012 N1-4).

3.1.2. Description of individual supercycles

Let us now examine the outburst behavior of individual supercycles. Here we define the identification of a supercycle by that of the starting superoutburst in a supercycle, that is, “supercycle 2011 S1”, for instance, is a supercycle which begins with a superoutburst 2011 S1, and ends with 2011 S2. The duration of a superoutburst is defined as a period

Table 2. List of superoutbursts

ID	The starting date of superpoutburst (BJD-2400000)	The maximum date of (BJD-2400000)	The maximum magnitude	The length of supercycle (d)
2011 S1	55578*	-	12.6*	—
2011 S2	55622.0	55625.1	12.7	44
2011 S3	55671.9	55674.4	12.7	50
2012 S1	55927 [§]	55929 [§]	12.9	58 [†]
2012 S2	55981.3	55982.6	13.0	54
2012 S3	56033.8	56034.4	12.9	53
2012 S4	-	56088.9 [‡]	-	55

*Based on VSNET data
[§]The precise timing is unclear because of the scarcity of observations)
[†]The date of previous superoutburst is based on VSNET data.
[‡]The estimated time of maximum,
not the start of the outburst (due to the scarcity of observations)

from the time of maximum of the superoutburst to its end because the observations of rising stage were lacking in some cases.

Supercycle 2011 S1:

The superoutburst 2011 S1 was the first superoutburst when negative superhumps were first detected (Paper I). Time resolved observations started three days after the detection of the superoutburst. Unfortunately the rising part of this superoutburst was not observed and the existence of the positive superhumps in this superoutburst was not confirmed. However, we suspect that the positive superhumps must have appeared most likely in the earliest phase of this superoutburst.

The superoutburst lasted for probably 13–15 d. Two days after the end of the superoutburst, the next normal outburst (2011 N1-1) started. In this supercycle, this object showed four normal outbursts (BJD 2455592, 2455597, 2455604, and 2455615). Besides them, a mini-outburst with the amplitude of only 1 mag occurred (BJD 2455611). The length of the supercycle was 44 d.

Supercycle 2011 S2 and 2011 S3:

The superoutburst 2012 S2 started as a form of a normal outburst and the start of the outburst was BJD 2455622 and persisted for 16 d. On BJD 2455642, 14 d after the supermaximum, the declining of the brightness temporarily ceased and this object brightened by 0.5 mag. The superoutburst 2011 S3 is similar to 2012 S2.

Supercycle 2012 S0:

Three normal outbursts (BJD 2455900, 2455909, 2455919) were caught before the first superoutburst where the time resolved observations were performed in the 2012 season. According to monitoring observation reported to VSNET, the previous superoutburst (2012 S0) occurred around BJD 2455869.

Supercycle 2012 S1:

Because of the lack of observations, it is unclear when the superoutburst 2012 S1 decayed although the decline occurred between BJD 2455941 and 2455943. Considering the maximum of the superoutburst was around BJD 2455962, the duration of superoutburst was approximately 15 d.

Supercycle 2012 S2:

The superoutburst 2012 S2 is an interesting case since the superoutburst was triggered on the way of decaying of normal outburst (the upper diagram of figure 4). The duration of the superoutburst 2012 S2 was 14 d. After the superoutburst ended, this object showed four normal outbursts (BJD 2456051, 2456057, 2456063, 2456070, 2456081) occurred.

Supercycle 2012 S3:

The superoutburst 2012 S3 is a typical superoutburst, which has a “shoulder” at the beginning of the superoutburst (the lower diagram of figure 4), which was shown in Osaki, Kato (2013a). Despite of the lack of the time-resolved observations in the late stage of the superoutburst 2012 S3, the VSNET data shows that this object declined around BJD 2456048–2456049. Thus the duration of the superoutburst 2012 S3 was 14–15 d. After the superoutburst decayed, four or five normal outbursts (BJD 2456051, 2456057, 2456063, 2456070, and 2456081) are detected. However, the fifth normal outburst (BJD 2456081) may be a precursor outburst of the next superoutburst 2012 S4. However, at any rate, the definite property of these outbursts are not clear because of the lack of the observations. The property of next outburst (2012 S4) is also unclear for the same reason.

Table 3. List of normal outbursts

ID	Cycle length (d)	The starting date of outburst (BJD−2400000)	Maximum Magnitude
2011 N1-1	-	55592.2	13.6
2011 N1-2	5.7	55597.9	13.5
2011 N1-3	6.6	55604.5	13.4
2011 N1-4	6.6	55611.1	14.3
2011 N1-5	4.0	55615.1	13.3
2011 N2-1	-	55644.7	13.6
2011 N2-2	5.5	55650.2	13.4
2011 N2-3	6.7	55656.9	13.5
2011 N2-4	7.2	55664.1	13.2
2011 N3-1	-	55693.3	13.7
2011 N3-2	4.8	55698.1	13.6
2011 N3-3	7.4	55705.5	13.6 [§]
2011 N3-4	6.8	55712.3	13.4
2011 N3-5 [‡]	9.0 [§]	55721.3	13.2 [§]
2012 N0-1	-	55900.5	13.6
2012 N0-2	9.0	55909.5	13.5
2012 N0-3	9.5	55919.0	13.4
2012 N1-1	-	55946.3	13.9
2012 N1-2	5.9	55952.2	13.7
2012 N1-3	8.9	55961.1	13.8
2012 N1-4	8.0	55969.1	13.5
2012 N2-1	-	55998.8	13.5
2012 N2-2	5.9	56004.7	13.9
2012 N2-3	8.2	56012.9	13.9
2012 N2-4	9.3	56022.2	13.5
2012 N2-5	9.4	56031.6 [†]	13.5
2012 N3-1	-	56051.0*	13.7
2012 N3-2	6.4	56057.4*	13.8
2012 N3-3	6.5	56063.9*	13.7
2012 N3-4	6.7	56070.6*	13.7
2012 N3-5	11.3	56081.9*	14.2

^{||}The cycle length from the previous outburst to the current one
^{*}The estimated maximum time, not the start of the outburst (due to the scarcity of observations)
[†]Precursor outburst of the next superoutburst
[‡]Suspected superoutburst
[§]Not so confirmed

3.2. The Frequency of Normal Outbursts

The number of normal outbursts in a supercycle in 2011 and 2012 was found to be mostly four and sometimes five (table 1). The cases of five are exceptional and they will be discussed below. We reported in Paper I that the frequency of normal outbursts in the first supercycle of 2011 (i.e., 2011 S1) as lower than those found in previous observations of ER UMa and we suggested that the existence of negative superhumps (and so the existence of a tilted disk) might suppress frequent occurrence of normal outbursts. Zemko et al. (2013) pointed out that the number of normal outbursts in a supercycle of ER UMa varied between 4 and 6 for a long time scale and they also suggested that these differences are related to the appearance of the negative superhumps. As discussed in the next subsection, it has turned out that all supercycles of ER UMa observed in 2011 and 2012 were accompanied by the negative superhump and thus they were the type L-supercycles (see, (Osaki, Kato 2013a), for the definition of the type L- and type S-supercycles).

This trend did not change largely between two seasons. Although five normal outbursts were observed between 2012 S1 and S2, the superoutburst 2012 S2 occurred at the declining stage of the fifth normal outburst. Thus this normal outburst was a precursor of the next superoutburst. Another exception is 2011 N1-4, which will be discussed in the later subsection. Except for these cases, four normal outbursts were observed during one supercycle. The same

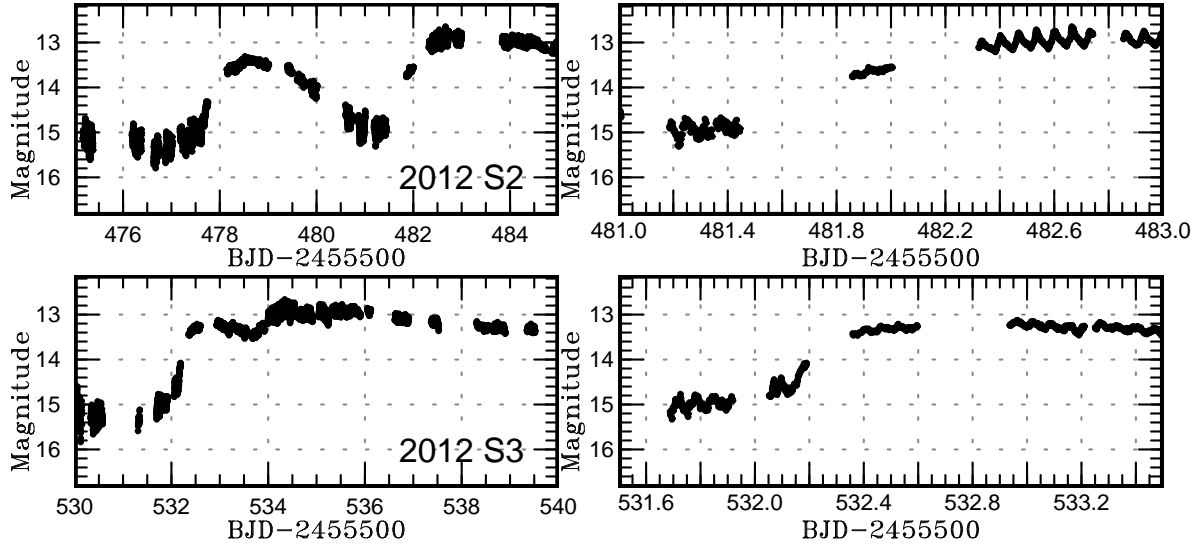


Fig. 4. Enlarged light curve of the rising stage of 2012 S2 (upper two panels) and 2012 S3 (lower two panels). The observation point is binned by 0.001 d. The left two panels show the precursors and the start of superoutbursts. And right two panels is further enlarged light curve in order to show the superhump variations. The positive superhumps became dimmed and the positive superhump evolved.

correlation between the appearance of negative superhumps and the frequency of normal outburst in a supercycle was known in other SU UMa stars, V503 Cyg (Kato et al. 2002, Pavlenko et al. 2012) and V1504 Cyg (Osaki, Kato 2013a). In this respect, Two exceptional cases of five normal outbursts in a supercycle are discussed here. As already mentioned in the individual supercycles, five normal outbursts occurred in supercycle 2012 S1 but the fifth one has turned out to be a precursor normal outburst of superoutburst 2012 S2 and it may be regarded as a part of the next superoutburst. Another exception is 2011 N1-4 and it was found to be a mini-outburst and it will be discussed in the later subsection.

3.2.1. Light Curve Profile and Rising Rate of Normal Outbursts in a Supercycle

Figure 5 illustrates variation in light curve profile of normal outbursts within supercycles. Figure exhibits the rising rates of normal outbursts within each supercycle. In the case of supercycle 2011 S1 (the left top panel of figure 5), we see that the rising rate to the maximum was getting slower with advance of supercycle phase except for the fifth one. We find from figure 5 that, generally speaking, the rising rate of the first normal outburst within each supercycle was faster than those is the light curves during of later ones. Two types of profiles in outburst light-curves are known to exist. The first one is that its rising rate is faster than its declining rate (i.e., rapid rise and slow decline) and the other one is that the rising rate to the maximum is not so fast but more or less similar to the decline rate (i.e., the light curve profile is more or less symmetric with respect to the rise and fall). In the disk instability model for the outburst of dwarf novae, the former type of light curve is produced by the “outside-in” type outburst (or the type A outburst in Smak (1984)) in which the transition to the hot state starts from the outer-part of the accretion disk and the heating front propagates inward while the latter type of outburst is produced by the “inside-out” outburst (type B in Smak (1984)) in which the transition to the hot state starts from the inner-part of the accretion disk. We find from these two figures that the first normal outburst in a supercycle looks like an “outside-in”-type, while most of other outbursts do like “inside-out”-type.

3.3. Negative superhumps

As shown in Paper I, negative superhumps are detected in ER UMa during superoutburst as well as during normal outbursts and quiescence. The negative superhumps were clearly detected except for the early stage of the superoutburst. Their amplitude is 0.5–1.0 mag in quiescence. We also show the amplitude variation in flux unit in figures 7, 8. In these diagram, 1 magnitude variation in 16 mag is normalized as 1. No dramatic change was associated with the change between quiescence and outburst is seen in flux unit (figures 7, 8) as already pointed in Osaki, Kato (2013a).

The valid interpretation for negative superhumps is the tilted accretion disk. The tilted disk show the retrograde precession, and Larwood (1998) presented a equation of q and ϵ_- for a retrograde precession of the tilted disk. According to Larwood (1998), the frequency of negative superhump frequency is given by

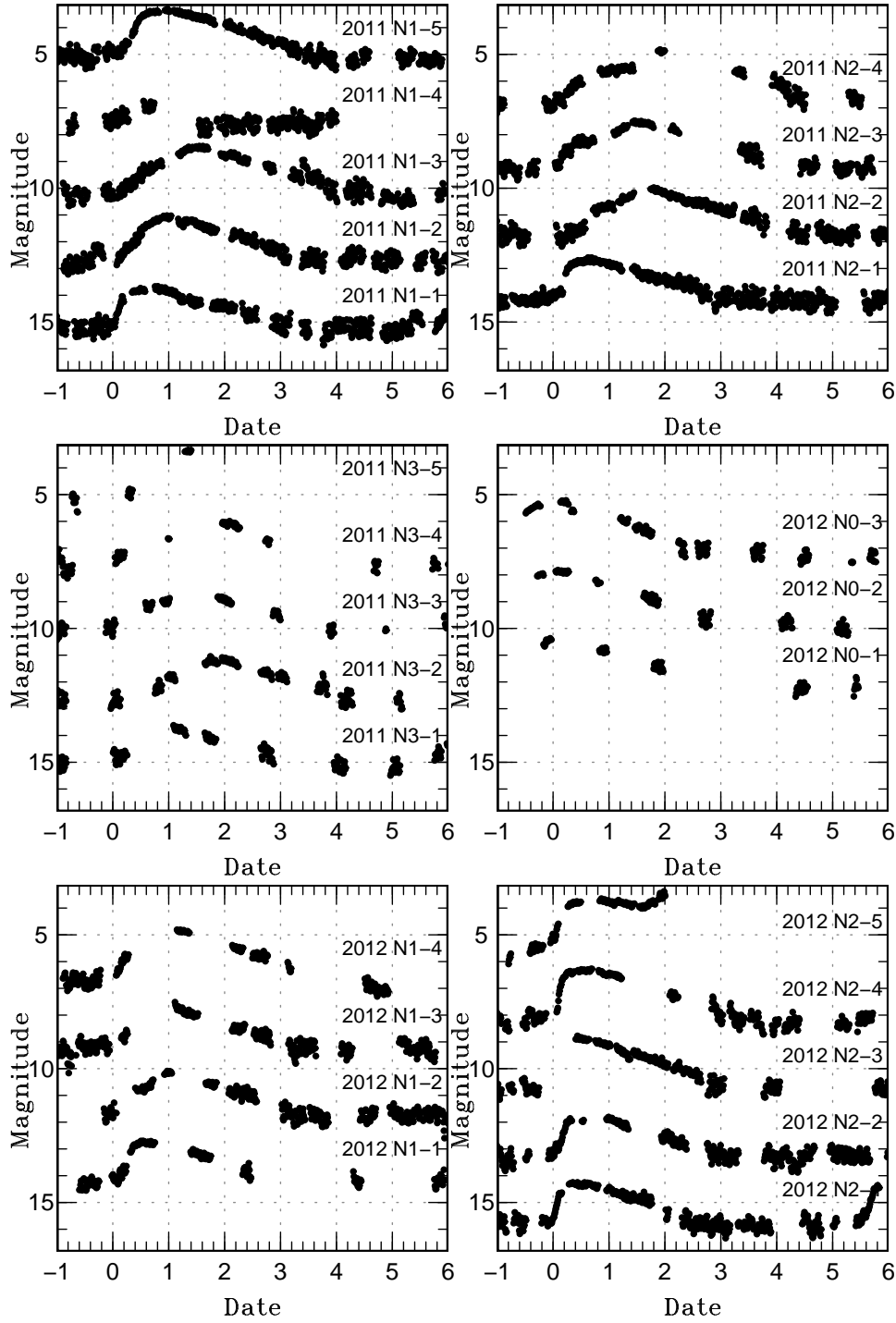


Fig. 5. Rising stage of normal outbursts. In the cycle of 2012 N0, the maximum of normal outbursts is set at zero, and in other cycles the start of normal outbursts is set at zero.

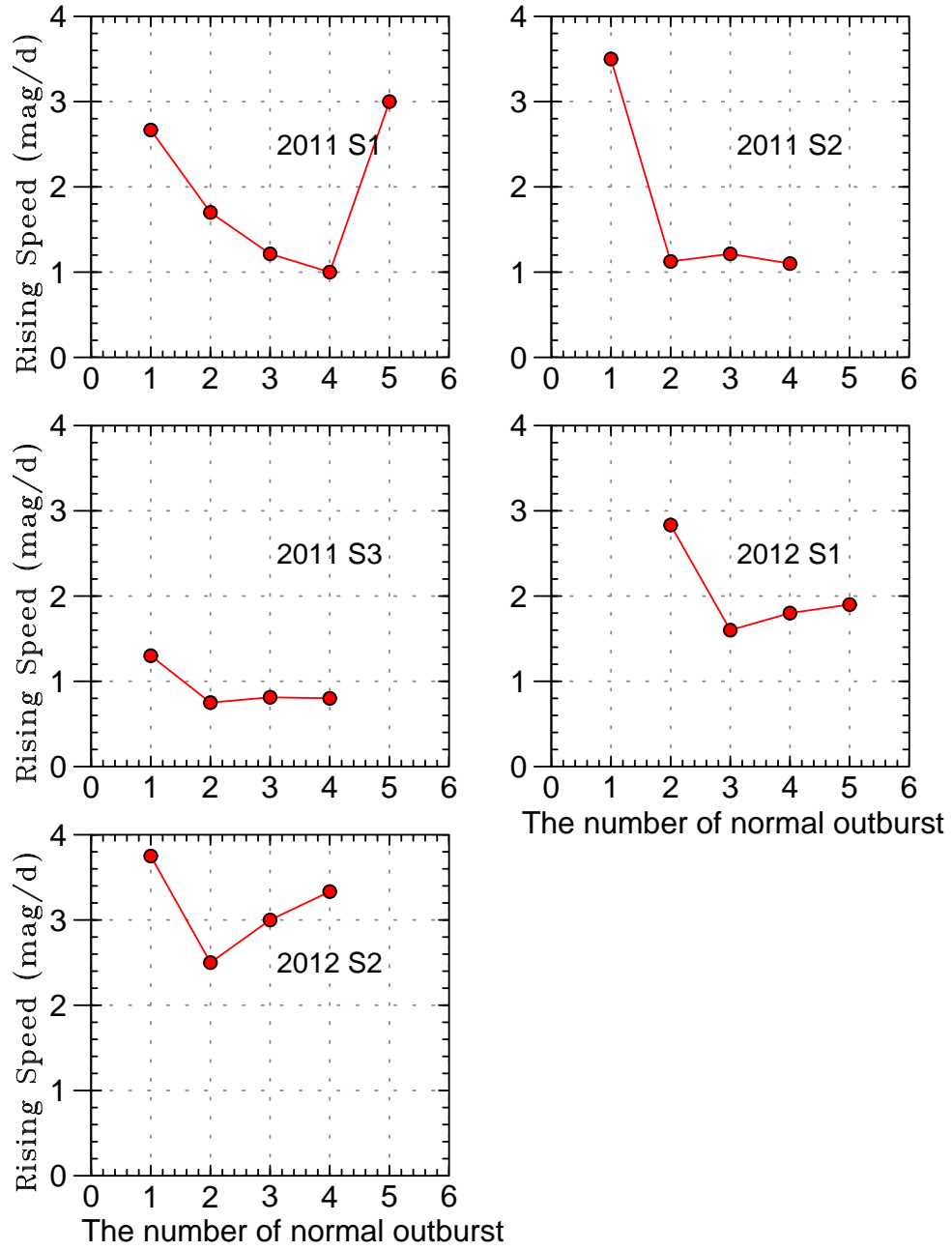


Fig. 6. Rising speed variation of each supercycle. Since the rising speed can be estimated because of the unclear timing of the start of outburst in some of normal outbursts, they are omitted.

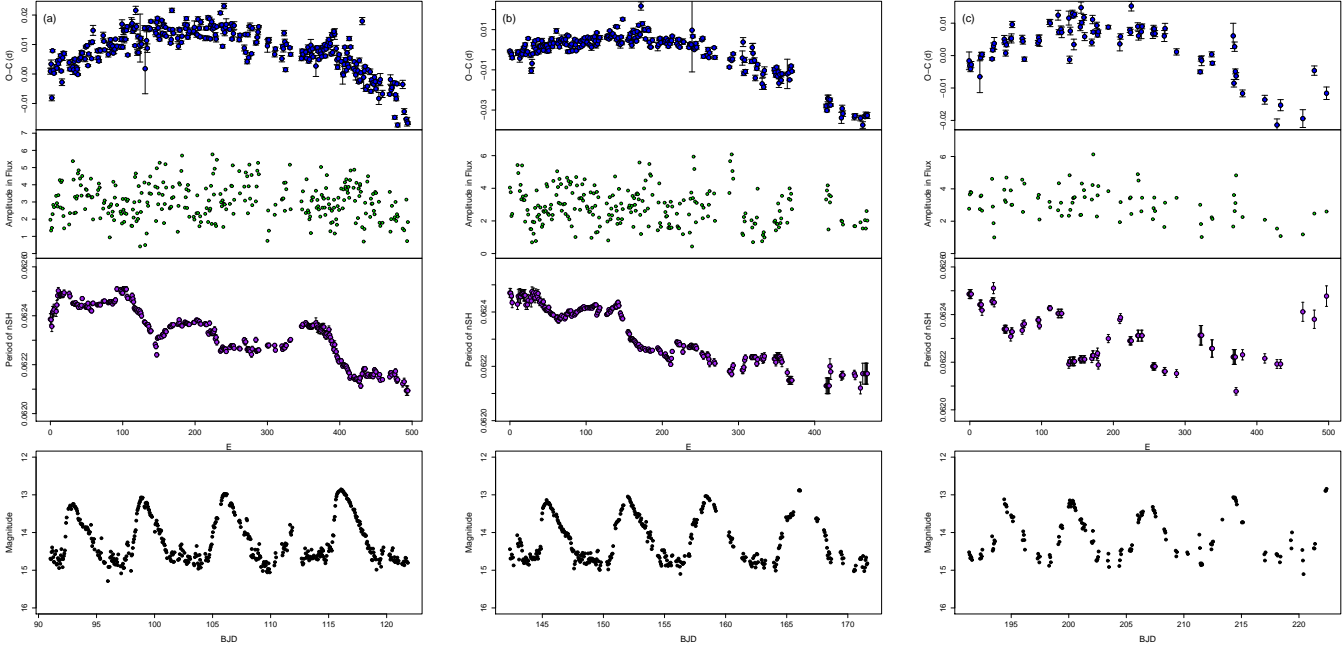


Fig. 7. $O - C$ diagram of negative superhumps, and related diagrams of during each supercycle of 2011. The panel of (a), (b), (c) correspond to supercycle 2011 S1, 2011 S2, and 2011 S3. For each panel, top to bottom: (1) $O - C$ diagram of negative superhumps, (2) The amplitude of negative superhumps in flux, (3) The period of negative superhumps estimate by PDM analysis, (4) The light curve. The $O - C$ value is against the equation of $2455591.020 + 0.062340E$. The middle panel shows diagrams during 2011 S2-S3. The $O - C$ value is against the equation of $2455642.346 + 0.062339E$. The lower panel shows diagrams between 2012 S3-4. The value is against the equation of $2455691.405 + 0.062305E$

$$\epsilon_{-}^{*} = \frac{\nu_{\text{orb}} - \nu_{\text{nSH}}}{\nu_{\text{orb}}} = -\frac{3}{7} \frac{q}{\sqrt{1+q}} \left(\frac{R_d}{A} \right)^{3/2} \cos \theta \quad (1)$$

, where ν_{orb} and ν_{nSH} are the frequency for negative superhumps and the orbital frequency of the binary, and θ is the tilt angle of the disk to the binary orbital plane. If θ is small, we can assume $\cos \theta \sim 1$ and ν_{nSH} can be determined by the disk radius R_d for specific system because q and A do not change in observational time-scale. In a real disk, $|\epsilon_{-}|$ represents the precession of the disk as a whole, to which precession rates from different radii contribute. Since the precession rates in smaller radii are smaller, the actual $-\epsilon_{-}$ is smaller than what is expected for a ring in the outer radius of the disk. For more details, see Appendix in Osaki, Kato (2013b).

Indeed Osaki, Kato (2013b) indicated that the frequency of negative superhump is useful probe to study the change of the radius of accretion disks in SU UMa-type dwarf novae through the analysis of V1504 Cyg. In this case, the frequency of negative superhumps varies systematically during supercycles and the variation of the frequency is a good probe of the variation of the disk. Now we can observe the persistent negative superhump of ER UMa. Thus We have a good opportunity to investigate the variation of the disk radius through the variation of negative superhump period.

We analyzed the period of negative superhumps in two methods. In subsection 3.3.1, we will take the periodic analysis with a traditional method in the research of dwarf novae, drawing $O - C$ diagrams. And in subsection 3.3.2, we will adopt a new method called least absolute shrinkage and selection operator (Lasso, Tibshirani 1996) and perform two dimensional spectral analysis.

3.3.1. $O - C$ analysis

We estimated the maximum timings of negative superhumps in the way given in Kato et al. (2009) for data except for superoutburst stage. The template for fitting the maximum was an average profile of negative superhump from data in quiescence between 2011 S1 and S2 (The period of used data for template are BJD 2455595–2455598, BJD 2455602–2455604.5, BJD 2455608–2455611, BJD 2455618–2455621, and these data is folded by the mean negative superhump period of these data, 0.0623106 d). We also estimated the amplitude of negative superhumps and showed in the same figure.

The resultant $O - C$ diagrams are figures 7, figure 8. The $O - C$ diagrams indicate that the period of negative superhump gradually shortens as the next superoutburst approaches. Namely the derivative of negative superhump period \dot{P}_{nSH} is negative between the successive superoutburst. The value of \dot{P}_{nSH} in 2011 is $-1.10(6) \times 10^{-5}$ (supercycle 2011 S1), $-1.32(4) \times 10^{-5}$ (supercycle 2011 S2), $-1.04(11) \times 10^{-5}$ (supercycle 2011 S3). Meanwhile the value of \dot{P}_{nSH} in 2012 is $-5(2) \times 10^{-6}$ (supercycle 2012 S0), $-9.7(4) \times 10^{-6}$ (supercycle 2012 S1), $-7.7(6) \times 10^{-6}$

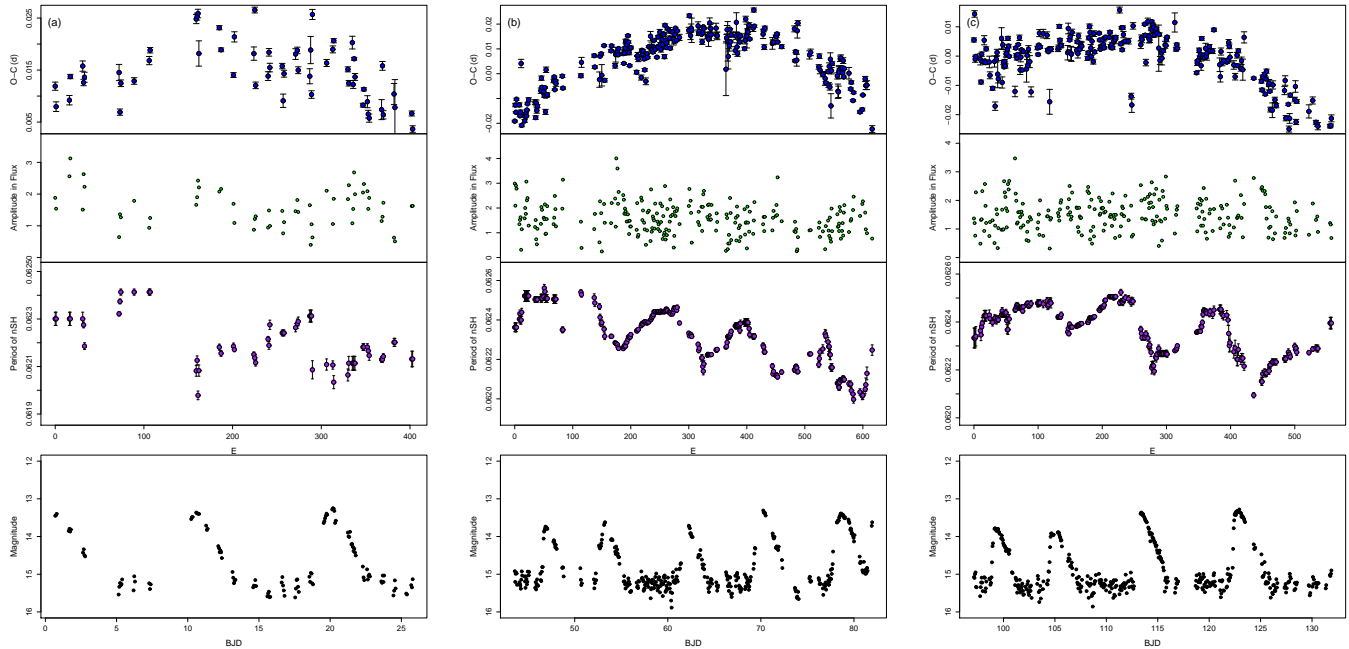


Fig. 8. $O - C$ diagram of negative superhumps, and related diagrams of during each supercycle of 2012. The panel of (a), (b), (c) correspond to supercycle 2012 S0, 2012 S1, and 2012 S2. For each panel, top to bottom: (1) $O - C$ diagram of negative superhumps, (2) The amplitude of negative superhumps in flux, (3) The period of negative superhumps estimated by PDM analysis, (4) The light curve. The $O - C$ value is against the equation of $2455900.680 + 0.06223E$. The upper right panel shows diagrams during supercycle 2012 S0. The $O - C$ value is against the equation of $2455943.576 + 0.0623E$. The lower panel shows diagrams between 2012 S1 and 2012 S2. The value is against the equation of $2455997.123 + 0.0624E$.

(supercycle 2012 S2). The absolute value of \dot{P}_{NSH} in 2011 is larger than that in 2012. However, the figure of $O - C$ diagram shown in figure 8 includes more complicated structures with shorter time-scales, or from the view of normal outburst cycle. Namely, these $O - C$ curves are composed of multiple curves of concave-up shape although the general appearance was concave down in long time-scale, namely from the view of supercycle. The third panel of figures 7, 8 is denoted to the change of period during each supercycle. These values were calculated by PDM analysis for a 5-d interval. Since the width is near the interval of normal outburst, it is hard to detect clear change of the period when interval of two normal outburst is short.

Since the period of the negative superhump is shorter than the orbital period, small period of negative superhumps corresponds to the large negative fractional superhump deficit ϵ_- . Thus this result implies that the absolute value of ϵ_- gradually increases as the next superoutburst approaches, and in shorter time-scale, the value of ϵ_- abruptly increases at the start of each normal outburst and gradually decreases until the next outburst starts. The increase of ϵ_- in the longer time-scale is because that the abrupt increase in the rising stage is larger than the gradual decrease in quiescence.

3.3.2. Lasso Period Analysis

Negative superhumps of ER UMa existed almost always during observations of 2011 and 2012. We made a detailed analysis for the frequency variations of negative superhumps. We computed two-dimensional power spectra of the light curve of ER UMa. We used locally weighted polynomial regression (LOWESS: Cleveland 1979) to the observation data in order to remove trends resulting from outbursts with R software². After that, we estimated the pulsed flux by multiplying the residual amplitudes and LOWESS-smoothed light curve converted to the flux scale. We used 10 d with of the moving window, and 1 d as the time step because the data is not as contiguous as Kepler data. Since the window length is longer than the normal outburst cycle, the periodic change of shorter time-scale is not well resolved. However, the periodic variation of longer time-scale is clearly seen.

We performed a period analysis called least absolute shrinkage and selection operator (Lasso, Tibshirani 1996), which was introduced to analysis of astronomical time-series data (Kato, Uemura 2012, Kato, Osaki 2013b). This method is very suitable to find peaks in power spectra and very strong method to analysis the rapid change of the period as in outbursting dwarf novae, because Lasso analysis has the advantage that peaks in power spectra are very sharp, and that it is less affected by uneven sampling data than Fourier analysis.

The resultant two-dimensional power spectra are shown in figures 9, 10. These figures show that the clear signal of

² <http://www.r-project.org/index.html>

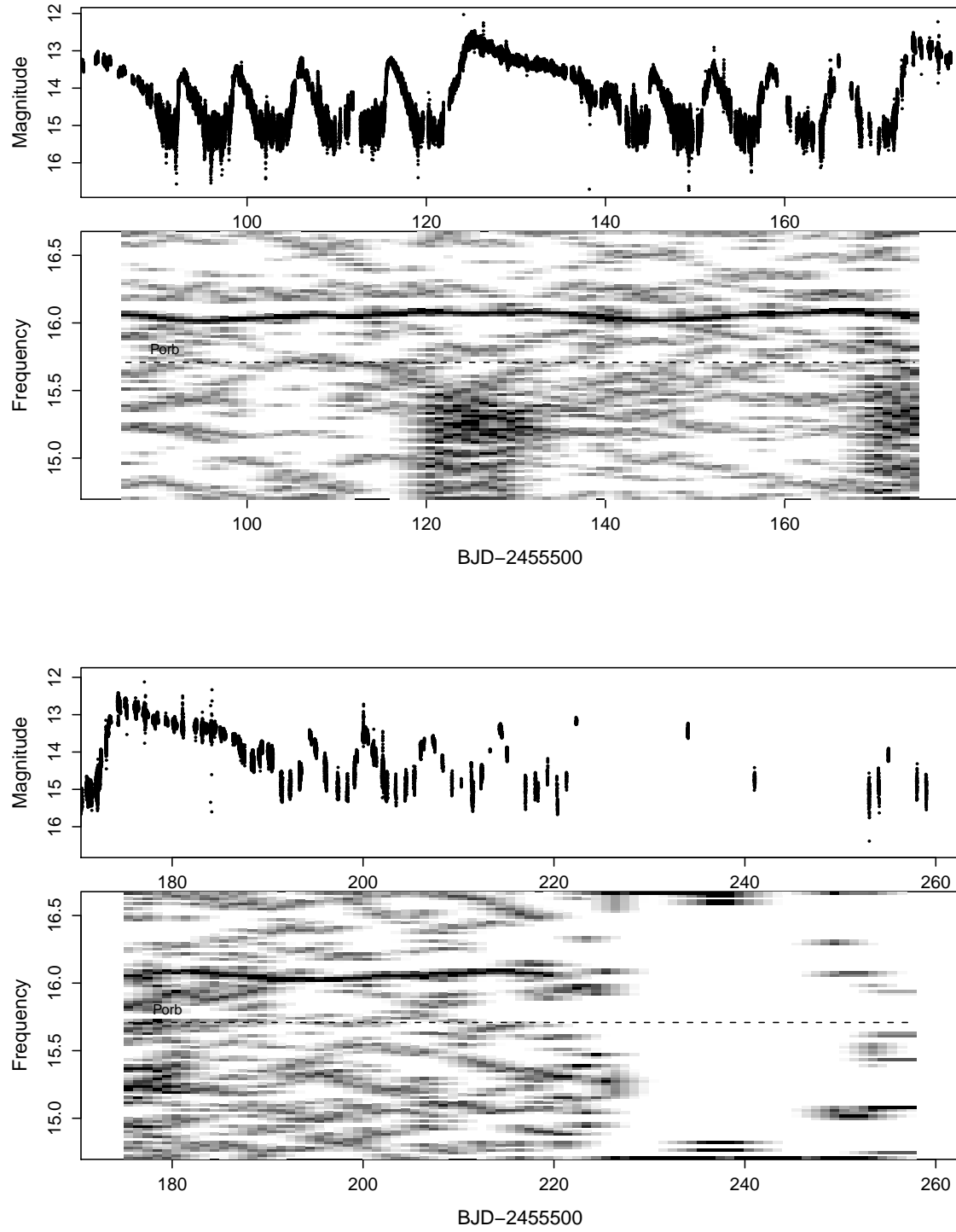


Fig. 9. Two dimensional period analysis of ER UMa using Lasso in 2011 season. For each two panels, the upper panel is the light curve and the lower panel is the power spectrum. The width of the window is 10 d, and the time step is 1 d.

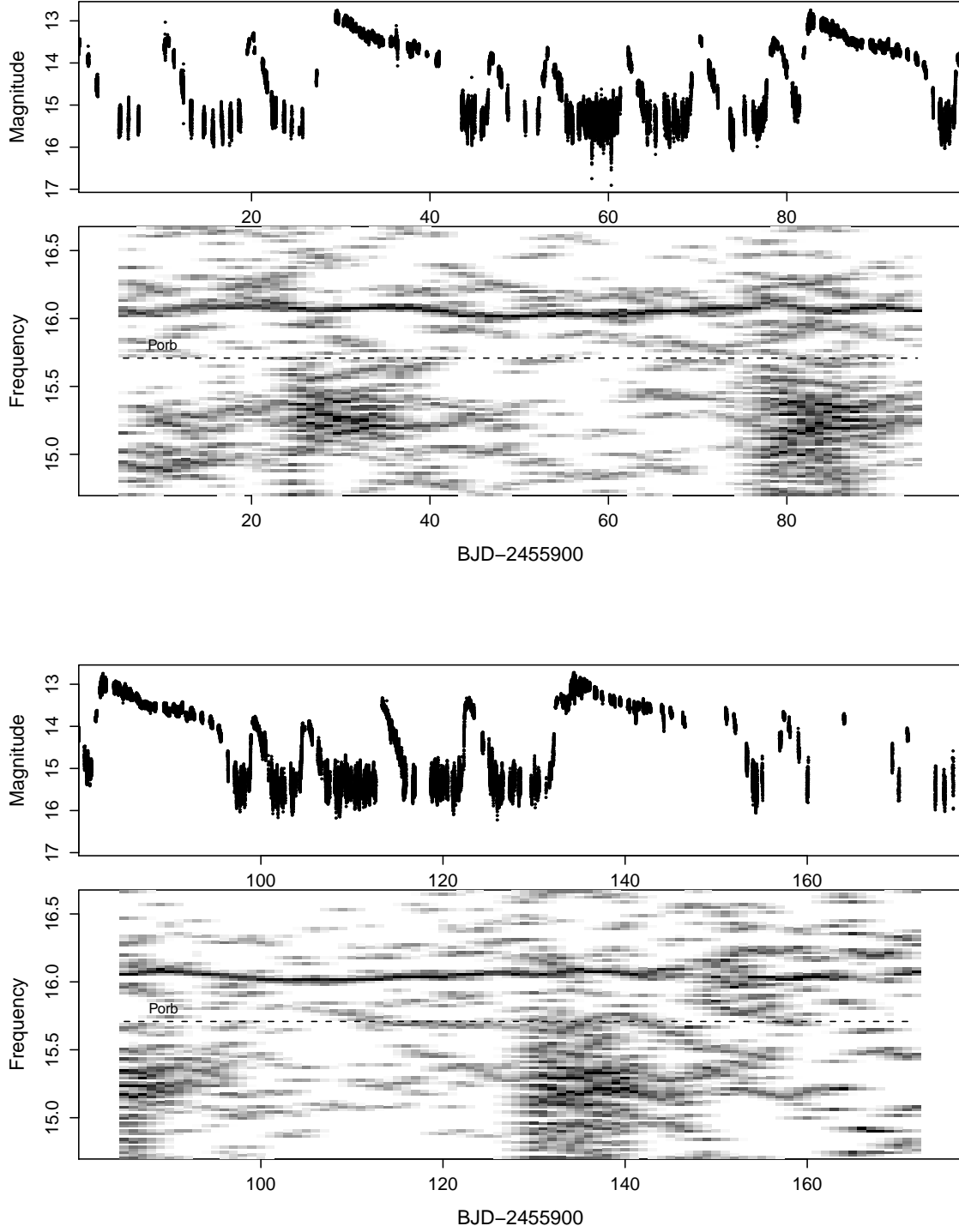


Fig. 10. Two dimensional period analysis of ER UMa using Lasso in 2012 season. For each two panels, the upper panel is the light curve and the lower panel is the power spectrum. The width of the window is 10 d, and the time step is 1 d.

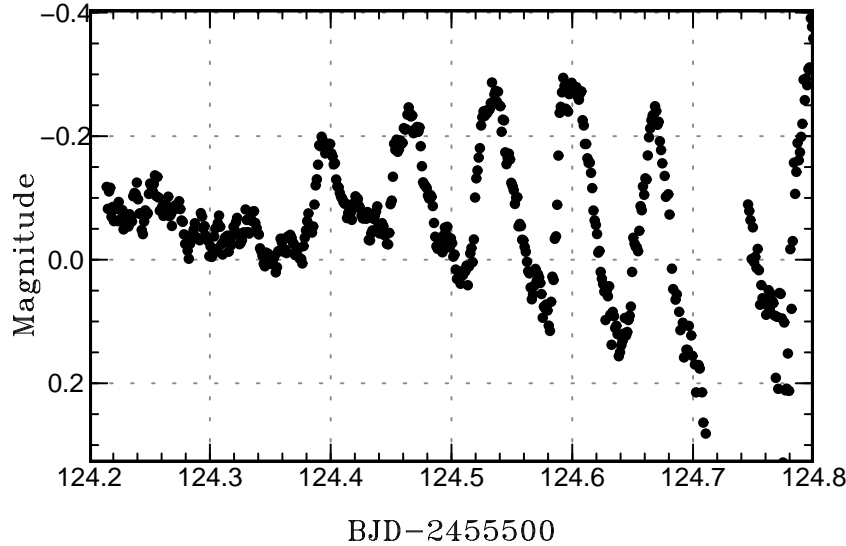


Fig. 11. Stage A superhump of 2011 S2. LOWESS fitting and the subtraction of negative superhump signal is already taken. The observed data is binned to 0.001 d.

negative superhump signal was always detected during two seasons, except for the early stage of superoutburst and later phase of 2011 season. Positive superhump signal was detected only in the early stage of superoutburst. The frequency of negative superhump changes during the supercycle. The frequency of negative superhump was smallest when the superoutburst ended and increases toward the next superoutburst.

Interestingly the Lasso diagram, especially in 2012 show orbital modulation is detected. Although we tried to the period of orbital modulation, significant signal is not seen because the signal was seen only partly.

Kato et al. (2013) and Osaki, Kato (2014) showed that the variation of negative superhump period in BK Lyn and ER UMa is not so large as that of ordinary SU UMa-type, such as V344 Lyr and V1504 Cyg and suggested this is because of the interval of these objects is extremely short.

3.3.3. The Discussion about the Periodic Variation in Negative Superhumps

Both the $O - C$ diagram and the Lasso analysis show that the negative superhump period shortens as the next superoutburst approaches in long time-scale. However, in short time-scale, the period of negative superhumps tends to become longer in quiescence and an abrupt shortening occurs at the start of normal outbursts. By the combination of these two effects, the period of negative superhump period becomes shorter as a whole accompanied by smaller variations coinciding with normal outbursts outside the superoutburst stage. This change corresponds to the global form of the $O - C$ diagram. The period change estimated by the PDM analysis is also in good agreement with this result.

The theoretical relation implies that the increase of ν_{nSH} can be interpreted as the increase of R_d/A . Thus the change of negative superhump period can be interpreted that the radius of the disk increases when the normal outburst is triggered and the accretion disk shrinks until the next normal outburst starts although the increase is larger than the decrease. This change of disk radius is similar that of V1504 Cyg shown in (Osaki, Kato 2013b, Osaki, Kato 2013b).

The TTI model suggests that the increase of disk radius at the start of outburst because of the conservation of angular momentum and the increased viscosity (Osaki 1989). After the outburst has finished, the disk radius shrinks until the next outburst starts. The negative superhump period becomes shorter as the next superoutburst approaches. Our result obeys this trend.

3.4. Positive superhump

3.4.1. The Stage A Superhumps

ER UMa also shows positive superhumps. In recent researches (e.g. Kato et al. 2009), a superoutburst can be divided to three stages named stage A, B, and C from the change of superhump period. Stage A corresponds to the evolving phase of superhump, when the tidal instability is limited within 3:1 resonance radius. After the superhumps after stage B, the eccentric wave spread to inner region of the disk and the pressure effect appears (Osaki, Kato 2013b). Thus stage A superhump period gives us the mass ratio q of the system (Kato, Osaki 2013a). It is very useful to detect stage A superhump and estimate the period.

Kato, Osaki (2013a) suggested an explanation why stage A superhumps are difficult to detect in ER UMa-type dwarf novae. In ER UMa-type dwarf novae, the superoutburst is not necessarily triggered by a normal outburst but

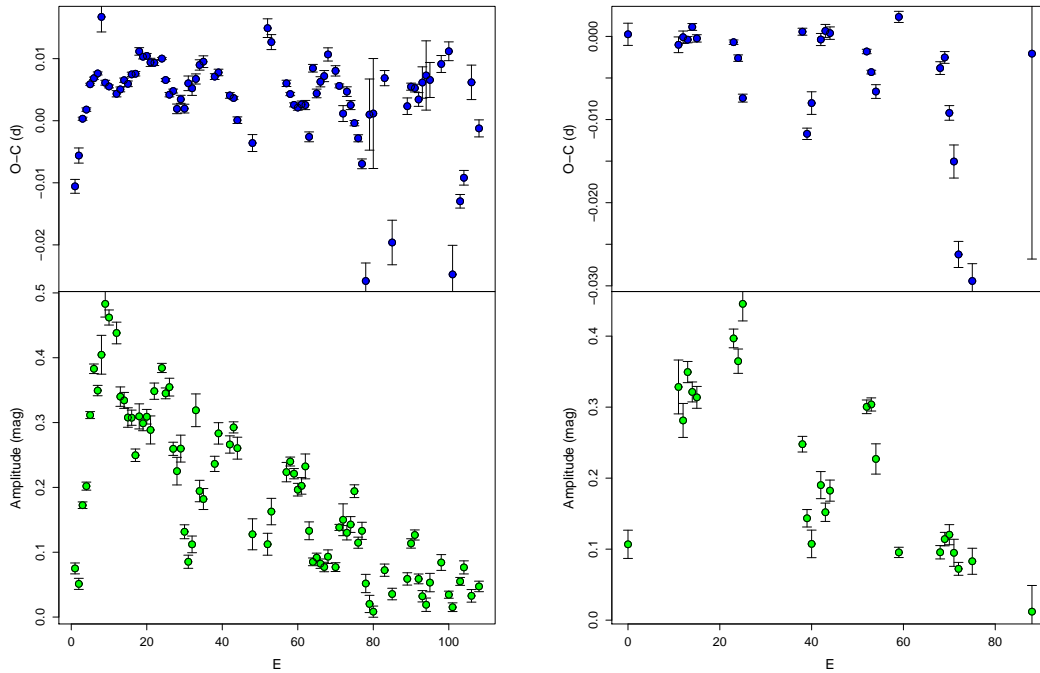


Fig. 12. $O - C$ diagrams of positive superhumps after subtracting negative superhumps of superoutbursts 2011 S2, S3. The $O - C$ values are against the equation of $2455624.392 + 0.065619E$ (for 2011 S2) and $2455674.280 + 0.065619E$ (for 2012 S3).

by the eccentric instability [called Case C outburst Osaki, Meyer (2003)]. In such case, the pressure effect has already been strong at the start of a superoutburst and the method to estimate q with stage A superhump period may not be applicable. However, in superoutbursts during our observations, positive superhumps were triggered by normal outburst as well as other usual SU UMa-type objects. Therefore the existence of the stage A superhump is expected.

As seen in figures 9 and 10, negative and positive superhumps co-exist during the superoutburst. It is supposed that positive superhump is caused by prograde precession of the elliptical disk and negative superhumps are caused by retrograde precession of the tilted disk. The co-existence of positive superhump and negative superhump suggests that the disk is eccentric and tilted at the same time.

This co-existence of negative and positive superhumps is a problem to estimate the maximum timings of positive superhumps. We have to subtract the variations of negative superhumps.

We adopted the averaged light curve of negative superhump used for the subtraction. First we subtracted from the original light curve translated to the flux scale. After that, the averaged light curve was formed data subset during one beat cycle. With this averaged light curve, After the subtraction, the scale was translated to the magnitude scale again. The subtracted light curve is figure 11.

After subtraction of negative superhumps, The $O - C$ diagrams of five superoutbursts are figures 12, 13. In 2011 S1, negative superhump was dominant at the start of time-resolved observation, thus $O - C$ curve of positive superhump could not be drawn.

Among five superoutbursts, stage A superhumps were detected in three superoutbursts (2011 S2, 2012 S2, and 2012 S3). These detection were based on the longer superhump period and the increase of the amplitude of superhumps in the earliest stage of the superoutburst. For instance, the amplitude of the positive superhumps evolved to 0.25 mag until $E = 10$ in 2011 S2 (figure 11). In 2011 S3 and 2012 S1, it was difficult to estimate stage A superhump period because of the lack of observation. After the amplitude of the positive superhumps reached the maximum, the amplitude of positive superhump became gradually smaller. These can be regarded as stage B superhumps. The perfect subtraction of negative superhump, especially in the later stage, is difficult, however. The profile of superhumps of ER UMa during superoutburst does not seem to be simple superposition of positive and negative superhumps.

We then obtained the periods of stage A superhumps. For the data of 2011 S2, A PDM analysis yielded a stage A superhump period of 0.06604(9) d. Similarly the stage A superhump period is estimated as 0.06570(2) d in 2012S2 and 0.06624(4) d in 2012 S3. With this data, the estimated q is 0.100(6) by the method of Kato, Osaki (2013a). Data of other superoutbursts show somewhat different value, 0.088 (2012 S2) and 0.114 (2012 S3). Using an average of these values, we adopted q of ER UMa to be 0.100(15).

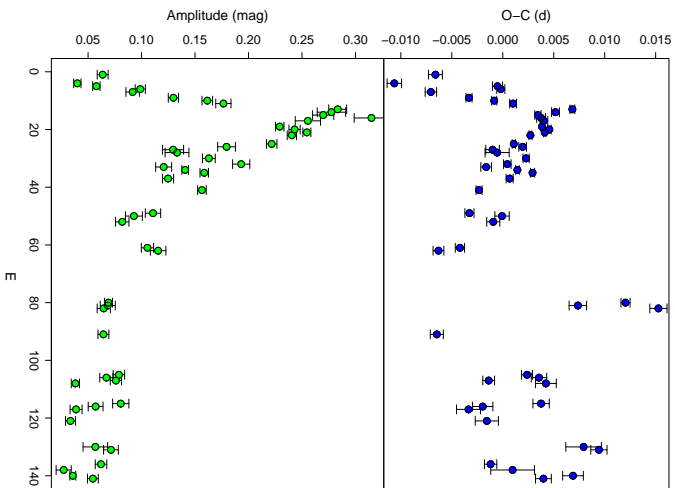
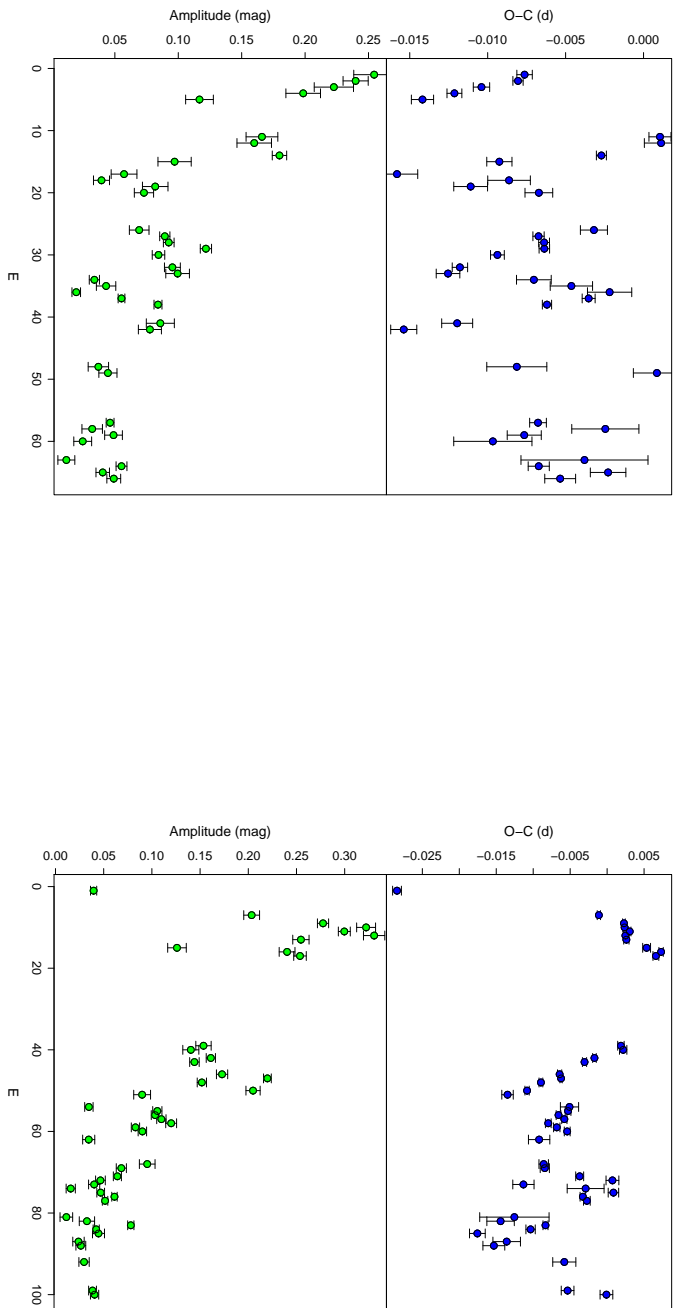


Fig. 13. $O - C$ diagrams of positive superhumps after subtracting negative superhumps of 2012 S1 – S3. The value is against the equation of $2.455924.094 + 0.065619E$ (for 2012 S1), $2.455982.403 + 0.065619E$ (for 2012 S2), $2.456034.104 + 0.065710E$ (for 2012 S3)

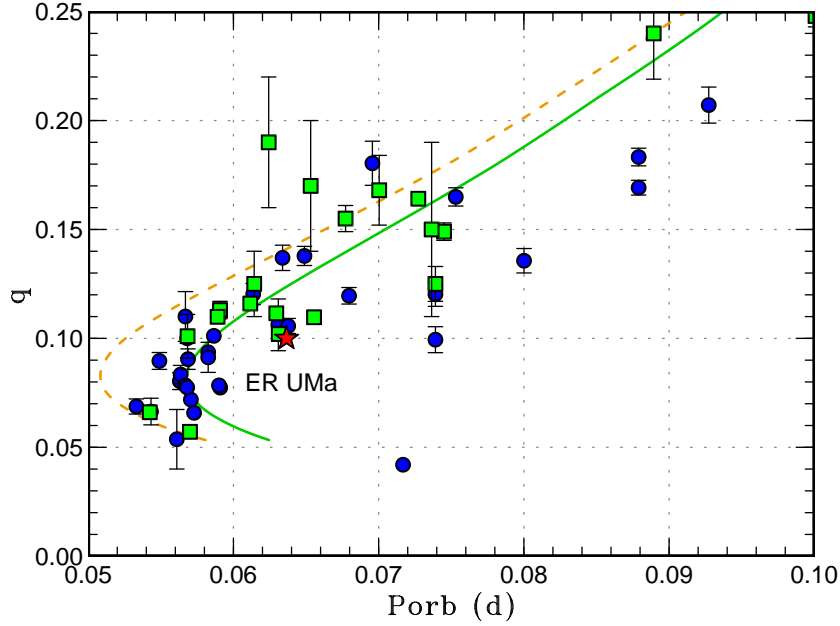


Fig. 14. Diagram of q versus P_{orb} . The data are derived from Kato, Osaki (2013a). The filled circles represent q estimated from stage A superhumps, filled squares represent q measured by eclipses. The filled star represents ER UMa. The dash curved line and solid curved line represent evolutionary track of the standard evolutionary theory and that of the modified evolutionary theory (Knigge et al. 2011).

3.4.2. System Property and Evolutionary State

The estimated value of q , 0.100(15) suggests that ER UMa is on the standard evolutionary track in Knigge et al. (2011) since the orbital period is 0.06366 d. Our results indicate that there is no evidence that ER UMa is in the evolutionary stage different from ordinary CVs although \dot{M} of ER UMa is much higher than other SU UMa-type dwarf novae with similar orbital periods.

Hellier (2001b) suggested that the unusual behavior of ER UMa-type (rapid recurrence of normal outbursts) or WZ Sge-type objects (rebrightenings) may be explained if these objects have extremely low q (i.e. near the period minimum or period bouncers) and the thermal and tidal instabilities are decoupled due to the weak tidal force. Our present result indicates that at least ER UMa itself is not the case. We consider that there is no necessity to consider decoupling of the thermal and tidal instabilities for ER UMa as shown by Osaki (1995a), in which the behavior of ER UMa can be reproduced by increasing the \dot{M} , while there remains a possibility for RZ LMi (Osaki 1995b). Determination of the orbital period and detection of stage A superhumps for RZ LMi and DI UMa are desired to solve this problem.

3.4.3. The relation between Positive and Negative Superhumps

The left panel of figure 15 shows the relation between the negative superhump period and the positive superhump period for systems which show both superhumps. Theoretically, the ratio the negative superhump period to the positive superhump period is 4/7 when the pressure effect does not effect. Most of that of systems obeys this relation. Among systems deviating from the theoretical relation, KIC 8751494 can be explained by the pressure effect Kato, Maehara (2013). The negative superhump of V1159 Ori may be not true negative superhumps, but “impulsive negative superhumps” (Osaki, Kato 2013b)³.

Our value of ER UMa is especially consistent with this relation. Although Gao et al. (1999) is far shorter than our value and theoretical prediction, this may also be an “impulsive negative superhump”. The right panel of figure 15 shows the relation between the orbital period and the negative superhump deficit.

3.5. The Transition from Negative Superhump to Positive Superhump

In paper I, we reported that the the maximum timings of negative and positive superhumps developed continuously and there was no phase shift between them. Paper I suggested that it implies the source of negative and positive superhumps is the same. The similar trend was seen also in other rising stages. However, this is unclear because the amplitude of superhumps in transition stage was small. We tested this suggestion in model calculations.

³ This phenomenon was also described in Wood et al. (2011).

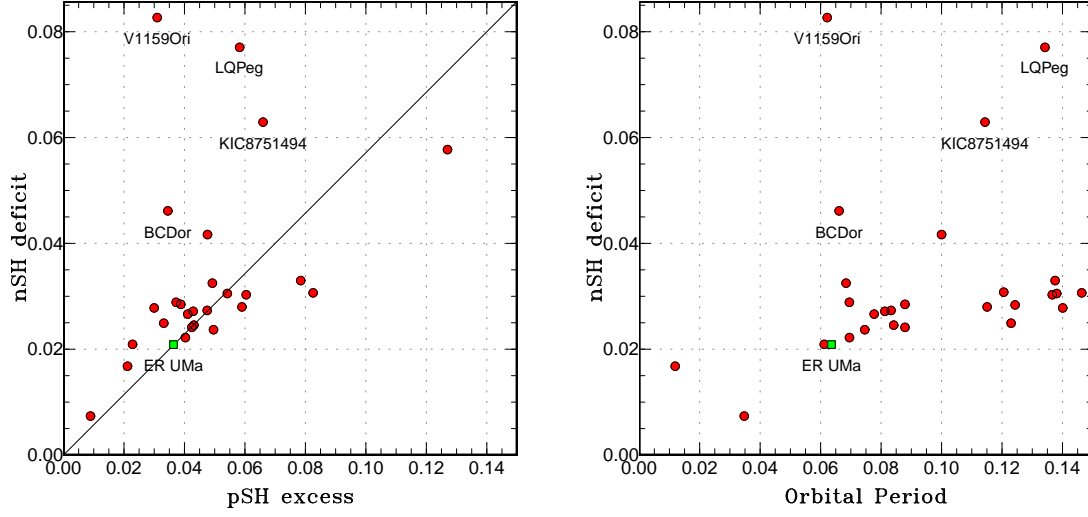


Fig. 15. ϵ_+ vs. ϵ_- diagram. The solid line implies that the theoretical predicted relation in the absence of the pressure effect. Reference: V1159 Ori (Patterson et al. 1995), AM CVn (Skillman et al. 1999, Patterson 1998, Patterson 1999), PX And (Stanishev et al. 2002), TV Col (Retter et al. 2003), BF Ara (Kato et al. 2003, Olech et al. 2007), V1405 Aql (Chou et al. 2001 Retter et al. 2002) AH Men (Patterson 1995), IR Gem (Fu et al. 2004), V503 Cyg (Harvey et al. 1995), TT Ari (Skillman et al. 1998, Andronov et al. 1999, Wu et al. 2002), V603 Aql (Patterson et al. 1997), RR Cha (Woudt, Warner 2002), V344 Lyr Still et al. 2010 (Osaki, Kato 2013b), V1504 Cyg (Osaki, Kato 2013b, Osaki, Kato 2013a), QU Aqr (Olech et al. 2009, Trampusch et al. 2005), BC Dor (Woudt et al. 2005), DW UMa (Stanishev et al. 2004, Patterson et al. 2005), V1974 Cyg (Olech 2002), KIC 8751494 (Kato, Maehara 2013), CSS 091121:033232+020439 (Woudt et al. 2012), KIC 7524178 (Kato, Osaki 2013b)

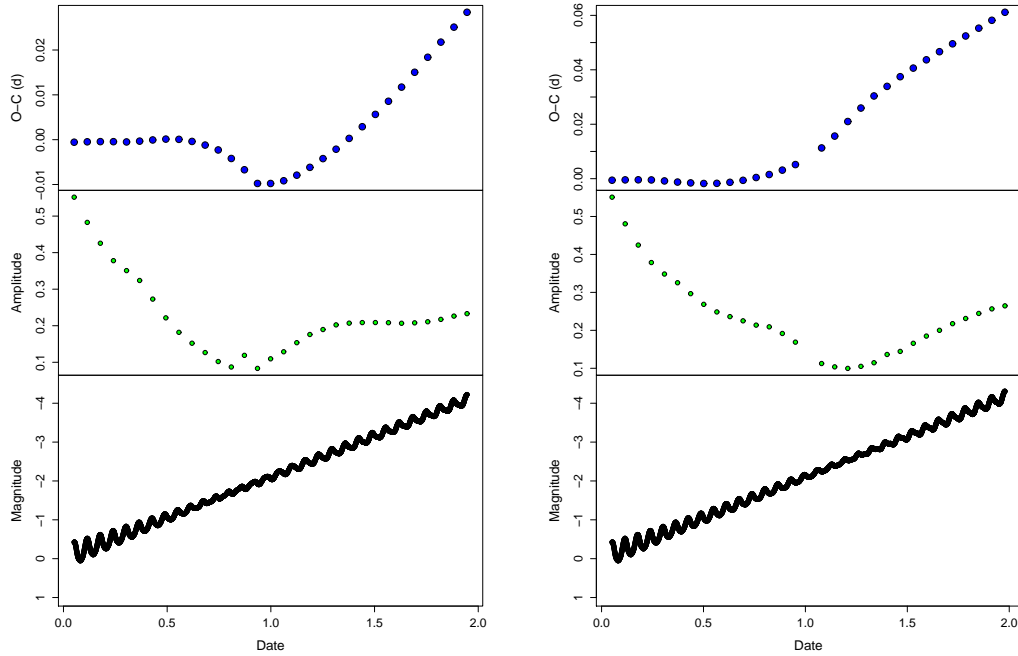


Fig. 16. Model calculation of the superimposition of negative and positive superhumps. In the left panel, the positive superhump starts at phase 0 when the phase of the negative superhump is also 0. In the right panel, the positive superhump starts at phase 0 when the phase of the negative superhump is 0.5. For each case, the variation of amplitude of hump and $O - C$ diagram at the transition stage from positive to negative superhump is shown.

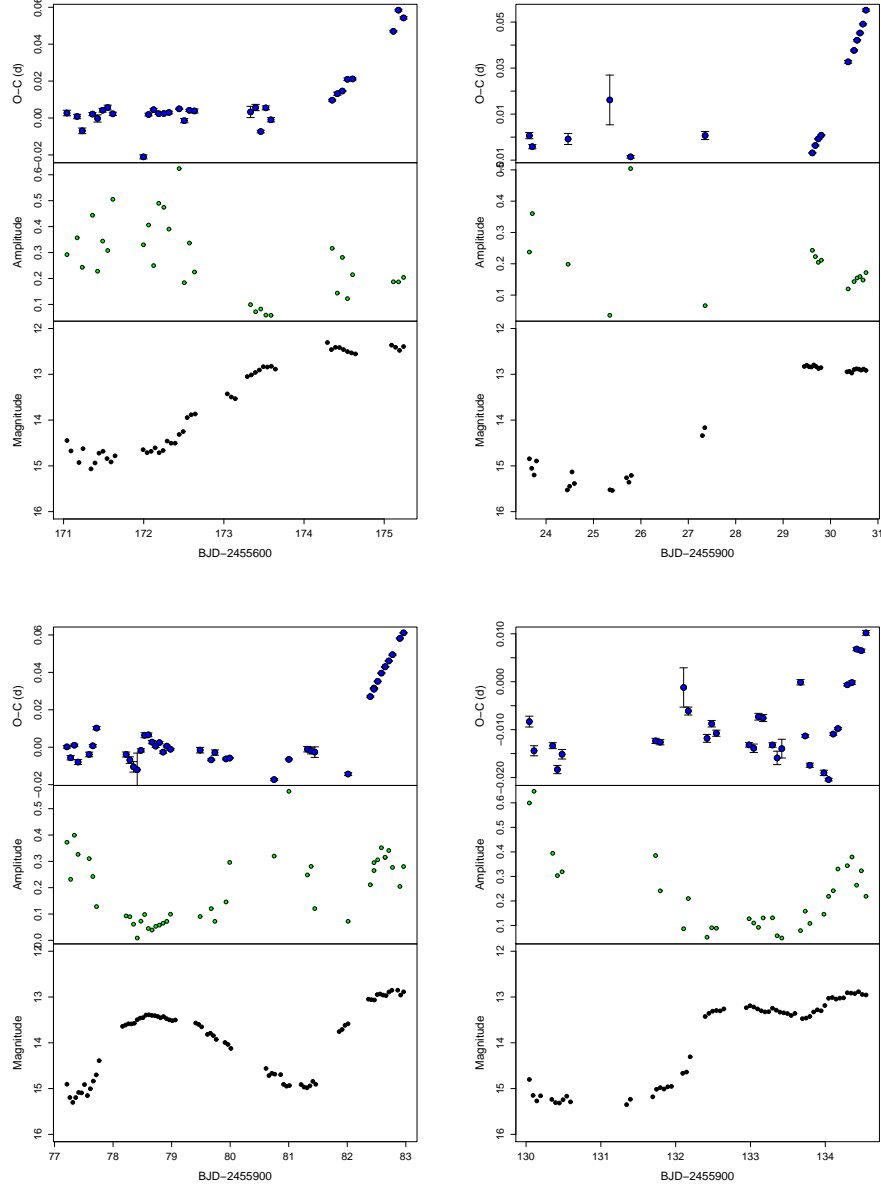


Fig. 17. $O - C$ diagrams, amplitude variation, and the light curve (0.01 d-binned) during the rising stage of superoutbursts. The upperleft panel is the diagram of the superoutburst 2011S3. The values of $O - C$ diagram is against the equation of $2455671.039 + 0.0622E$. The upperright panel is the diagram of the superoutburst 2012S1. The values of $O - C$ diagram is against the equation of $2455923.646 + 0.0622E$. The bottomleft panel is the diagram of the superoutburst 2012S2. The values of $O - C$ diagram is against the equation of $2456077.211 + 0.0622E$. The bottomright panel is the diagram of the superoutburst 2012S3. The values of $O - C$ diagram is against the equation of $245630.052 + 0.0622E$. For 2011S1, see fig 3 of Paper I. These diagrams suggests

We assumed the positive superhump develops in the rising stage of the superoutburst and the constant amplitude in flux of negative superhump, 0.7 mag in quiescence. The rising rate of mean magnitude is 2.1 mag / d. Positive superhumps start the development four cycles after the rising starts. After positive superhumps appearing, the amplitude of positive develops at the speed of 0.15 mag /d. For the profile of negative and positive superhumps, the template profiles used for non-linear fitting were adopted.

The resultant diagrams are shown in figure 16. In the upper diagram, the phases of negative and positive superhump are continuous when the positive superhumps start to develop. In the lower diagram, the phases of negative and positive superhump are different by 0.5. The both diagrams both show the decrease of the amplitude of variation when the positive superhumps begin to develop. Furthermore, the negative superhump phase evolve into the positive superhump smoothly in the both $O-C$ diagrams. In the upper panel of figure 16, $O-C$ variation does not show small a smooth transition from negative superhump to positive superhump, but shows more complex structure. This is caused by the superimposition of the maxima of negative and positive superhump. However, since the amplitude of positive superhump is small, the shift of $O-C$ value is small.

The $O-C$ diagrams of the rising stage of each superoutburst is shown in figure 17. These $O-C$ diagrams imply that the negative and positive superhumps are continuous without phase shift as in the lower case of figure 16. This result suggests that the position where the positive superhump is not randomly excited in relation to negative superhumps.

This result would not be expected if the negative superhumps arise from the varying release of the potential energy on a tilted disk and the phase of the tilt is random to the observer when positive superhumps start to grow. Either our understanding of the origin of negative superhumps may be insufficient or the statistics may not sufficient to prove whether the positive superhump is randomly excited in relation to negative superhumps. Further systematic observations of the rising stage of superoutbursts are required.

4. Conclusion

We observed the SU UMa-type dwarf nova ER UMa in the years 2011 and 2012 by VSNET worldwide campaign and we obtained data of 307 nights spanning in 2011 – 2012. We detected persistent negative superhumps during the superoutbursts as well as during normal outbursts and quiescence in both seasons. We analyzed these data and obtained the following are our major findings:

(1) We succeeded in covering three supercycles of this star in 2011 and also three supercycles in 2012. The star showed persisted superhumps in both seasons.

(2) We analyzed periodic variations of negative superhumps in a supercycle of this star by $O-C$ analysis, PDM analysis, and Lasso analysis. We have found from these analyses that the period of negative superhumps between two successive superoutbursts decreases secularly from the end of a superoutburst to the next superoutburst in a longer time-scale of a supercycle. Superimposed on this long time-scale trend, a shorter time-scale variation in the negative superhump period occurred within a normal outburst cycle in a sense that the period was shortened when a normal outburst occurred and it became longer during quiescence. When the next supercycle started, the period of negative superhumps returned to the value when the previous supercycle started. Thus it varied cyclically with the same supercycle period as that of the light curve. This variation was indicates as a result of the variation in the disk radius and the disk radius was the smallest at the end of a superoutburst. The variation in the disk radius inferred by our analysis of ER UMa is in agreement with the predicted variation of the disk radius by the TTI theory.

(3) The rising rate of maximum of the normal outburst varied during one supercycle. The rising rate of the first normal outburst within a supercycle was found to be faster than the later ones. This suggests that the first normal outburst may most likely be of the “outside-in” type while the later ones may be of the “inside-out” type. The occurrence of the “inside-out”-type outbursts in ER UMa may be understood as due to the mass supply from the secondary to the inner part of the disk when the disk tilted.

(4) The negative superhumps and the positive superhumps co-existed during the superoutburst although the signal of the negative superhump was marginal in the first several days of the superoutburst. By subtracting the signal of negative superhumps, we obtained the $O-C$ diagram for the positive superhumps and by doing so we were able to distinguish the stage A from the B ones. A simple combination of the positive and negative superhumps was not sufficient to reproduce the complex profile variation.

(5) The number of normal outbursts in a supercycle of ER UMa in 2011 and 2012 was found to be mostly four, which was smaller than that in other occasions when negative superhumps were not observed, a result consistent with those reported for ER UMa by Zemko et al. (2013) and for V1504 Cyg by Osaki, Kato (2013a). This can be understood as a result of the tilted disk: when the disk is tilted, the gas stream coming from the secondary arrives at the inner region of the disk rather than at the disk edge and this reduces a frequent occurrence of the outside-in type normal outbursts.

(6) Some of the superoutbursts were triggered by the normal outbursts (i.e. precursor outbursts). Positive superhumps started to grow during the declining part of the precursor in such superoutbursts. The phases of maxima were found to be continuous when a transition from the negative superhump to the positive superhump occurred.

(6) We succeeded in detecting stage A superhumps for the first time in ER UMa-type dwarf novae during the precursor parts of three superoutburst. Using the period of stage A superhumps, we estimated q of ER UMa to be 0.100(15). The estimated q and the known orbital period imply that ER UMa itself is in the standard evolutionary track of cataclysmic variable stars. However, the mass transfer rate, \dot{M} of ER UMa, inferred from its short supercycle length and frequent occurrence of normal outbursts, is much higher than that of other SU UMa-type dwarf novae with similar orbital periods.

The authors are grateful to observers of VSNET Collaboration and VSOLJ observers, who contributed observations, covering long-term variations of ER UMa as long as two years.

This work was partly supported by the Grant-in-Aid “Initiative for High-Dimensional Data-Driven Science through Deepening of Sparse Modeling” from the Ministry of Education, Culture, Sports, Science and Technology (MEXT) of Japan, and Grants-in-Aid for the Global COE Programme “The Next Generation of Physics, Spun from Universality and Emergence” from the Ministry of Education, Culture, Sports, Science and Technology of Japan. We are very grateful to the referee of this paper, Osaki, Y.

Appendix 1. The list of all observations

Appendix 2. The maximum timings of negative superhumps

References

- Andronov, I. L., et al. 1999, *AJ*, 117, 574
- Chou, Y., Grindlay, J. E., & Bloser, P. F. 2001, *ApJ*, 549, 1135
- Cleveland, W. S. 1979, *J. Amer. Statist. Assoc.*, 74, 829
- Fu, H., Li, Z.-Y., Leung, K.-C., Zhang, Z.-S., Li, Z.-L., & Gaskell, C. M. 2004, *Chinese J. Astron. Astrophys.*, 4, 88
- Gao, W., Li, Z., Wu, X., Zhang, Z., & Li, Y. 1999, *ApJL*, 527, L55
- Harvey, D., Skillman, D. R., Patterson, J., & Ringwald, F. A. 1995, *PASP*, 107, 551
- Hellier, C. 2001a, *Cataclysmic Variable Stars: How and why they vary* (Berlin: Springer-Verlag)
- Hellier, C. 2001b, *PASP*, 113, 469
- Hirose, M., & Osaki, Y. 1990, *PASJ*, 42, 135
- Kato, T., Bolt, G., Nelson, P., Monard, B., Stubbings, R., Pearce, A., Yamaoka, H., & Richards, T. 2003, *MNRAS*, 341, 901
- Kato, T., et al. 2013, *PASJ*, in press (arxiv/1310.7069)
- Kato, T., et al. 2009, *PASJ*, 61, S395
- Kato, T., Ishioka, R., & Uemura, M. 2002, *PASJ*, 54, 1029
- Kato, T., & Kunjaya, C. 1995, *PASJ*, 47, 163
- Kato, T., & Maehara, H. 2013, *PASJ*, 65, 76
- Kato, T., Nogami, D., Baba, H., Masuda, S., Matsumoto, K., & Kunjaya, C. 1999, in *Disk Instabilities in Close Binary Systems*, ed. S. Mineshige, & J. C. Wheeler (Tokyo: Universal Academy Press), 45
- Kato, T., & Osaki, Y. 2013a, *PASJ*, 65, 115
- Kato, T., & Osaki, Y. 2013b, *PASJ*, 65, L13
- Kato, T., & Uemura, M. 2012, *PASJ*, 64, 122
- Kato, T., Uemura, M., Ishioka, R., Nogami, D., Kunjaya, C., Baba, H., & Yamaoka, H. 2004, *PASJ*, 56, S1
- Kjurkchieva, D., & Marchev, D. 2010, *Publ. Astron. Obs. Belgr.*, 90, 147
- Knigge, C., Baraffe, I., & Patterson, J. 2011, *ApJS*, 194, 28
- Larwood, J. 1998, *MNRAS*, 299, L32
- Nogami, D., Kato, T., Masuda, S., & Hirata, R. 1995, *Inf. Bull. Variable Stars*, 4155
- Ohshima, T., et al. 2012, *PASJ*, 64, L3
- Olech, A. 2002, *Acta Astron.*, 52, 273
- Olech, A., Rutkowski, A., & Schwarzenberg-Czerny, A. 2007, *Acta Astron.*, 57, 331
- Olech, A., Rutkowski, A., & Schwarzenberg-Czerny, A. 2009, *MNRAS*, 399, 465
- Osaki, Y. 1989, *PASJ*, 41, 1005
- Osaki, Y. 1995a, *PASJ*, 47, L11
- Osaki, Y. 1995b, *PASJ*, 47, L25
- Osaki, Y. 1996, *PASP*, 108, 39
- Osaki, Y., & Kato, T. 2013a, *PASJ*, 65, 50
- Osaki, Y., & Kato, T. 2013b, *PASJ*, in press (arxiv/1305.5877)
- Osaki, Y., & Kato, T. 2014, *PASJ*, in press (arxiv/1309.3722)
- Osaki, Y., & Meyer, F. 2003, *A&A*, 401, 325
- Patterson, J. 1995, *PASP*, 107, 657
- Patterson, J. 1998, *PASP*, 110, 1132
- Patterson, J. 1999, in *Disk Instabilities in Close Binary Systems*, ed. S. Mineshige, & J. C. Wheeler (Tokyo: Universal Academy Press), 61
- Patterson, J., Jablonski, F., Koen, C., O’Donoghue, D., & Skillman, D. R. 1995, *PASP*, 107, 1183
- Patterson, J., et al. 2005, *PASP*, 117, 1204
- Patterson, J., Kemp, J., Saad, J., Skillman, D. R., Harvey, D., Fried, R., Thorstensen, J. R., & Ashley, R. 1997, *PASP*, 109, 468
- Pavlenko, E. P., Samsonov, D. A., Antonyuk, O. I., Andreev, M. V., Baklanov, A. V., & Sosnovskij, A. A. 2012, *Astrophysics*, 55, 494
- Retter, A., Chou, Y., & T., Bedding 2002, in *ASP Conf. Ser.* 261, *The Physics of Cataclysmic Variables and Related Objects*, ed. B. T. Gänsicke, K. Beuermann, & K. Reinsch (San Francisco: ASP), 527
- Retter, A., Hellier, C., Augusteijn, T., Naylor, T., Bedding, T. R., Bembrick, C., McCormick, J., & Velthuis, F. 2003, *MNRAS*, 340, 679
- Ringwald, F. A., Velasco, K., Roveto, J. J., & Meyers, M. E. 2012, *New Astron.*, 17, 433
- Robertson, J. W., Honeycutt, R. K., & Turner, G. W. 1995, *PASP*, 107, 443
- Skillman, D. R., et al. 1998, *ApJL*, 503, L67
- Skillman, D. R., Patterson, J., Kemp, J., Harvey, D. A., Fried, R. E., Retter, A., Lipkin, Y., & Vanmunster, T. 1999, *PASP*, 111, 1281
- Smak, J. 1984, *Acta Astron.*, 34, 161
- Smak, J. 1985, *Acta Astron.*, 35, 357
- Stanishev, V., Kraicheva, Z., Boffin, H. M. J., & Genkov, V. 2002, *A&A*, 394, 625

- Stanishev, V., Kraicheva, Z., Boffin, H. M. J., Genkov, V., Papadaki, C., & Carpano, S. 2004, *A&A*, 416, 1057
- Still, M., Howell, S. B., Wood, M. A., Cannizzo, J. K., & Smale, A. P. 2010, *ApJL*, 717, L113
- Tibshirani, R. 1996, *J. R. Statistical Soc. Ser. B*, 58, 267
- Tramposch, J., Homer, L., Szkody, P., Henden, A., Silvestri, N. M., Yirak, K., Fraser, O. J., & Brinkmann, J. 2005, *PASP*, 117, 262
- Udalski, A. 1988, *Acta Astron.*, 38, 315
- Warner, B. 1995, *Cataclysmic Variable Stars* (Cambridge: Cambridge University Press)
- Whitehurst, R. 1988, *MNRAS*, 232, 35
- Wood, M. A., & Burke, C. J. 2007, *ApJ*, 661, 1042
- Wood, M. A., Still, M. D., Howell, S. B., Cannizzo, J. K., & Smale, A. P. 2011, *ApJ*, 741, 105
- Woudt, P. A., & Warner, B. 2002, *MNRAS*, 335, 44
- Woudt, P. A., Warner, B., de Budé, D., Macfarlane, S., Schurch, M. P. E., & Zietsman, E. 2012, *MNRAS*, 421, 2414
- Woudt, P. A., Warner, B., & Spark, M. 2005, *MNRAS*, 364, 107
- Wu, X., Li, Z., Ding, Y., Zhang, Z., & Li, Z. 2002, *ApJ*, 569, 418
- Zemko, P., Kato, T., & Shugarov, S. 2013, *PASJ*, 65, 54

Table 4. Log of observation list

Start*	End*	N^{\S}	obs	sys [#]	exp
81.4612	81.7636	382	deM	C	60s
83.0675	83.3887	410	Aka	C	60s
83.9591	84.0043	100	Kra	-	30s
84.0048	84.0497	99	Kra	C	30s
84.0048	84.3783	888	Ioh	C	15s
84.6368	84.7775	306	Kra	C	30s
85.6340	86.0532	917	Kra	C	30s
86.0664	86.3767	421	Aka	C	60s
87.1712	87.3828	293	Aka	C	60s
87.7992	88.0526	549	Kra	C	30s
88.0493	88.3827	434	Aka	C	60s
88.7965	89.0512	401	Kra	C	50s
89.0715	89.3325	338	Aka	C	60s
89.7937	90.0516	406	Kra	C	50s
90.0890	90.3768	341	Aka	C	60s
90.1906	90.2003	15	Ioh	C	15s
90.2019	90.3130	437	KU	C	15s
90.4132	90.7707	447	deM	C	60s
90.7909	91.0508	409	Kra	C	50s
90.9506	91.3721	1011	Ioh	C	15s
91.0508	91.3786	441	Aka	C	60s 45s
91.1379	91.3305	111	OUS	C	60s
91.1400	91.3355	161	OUS	-	30s
91.1908	91.3808	808	KU	C	15s
91.5065	91.6415	232	Ter	C	45s
91.5456	91.7274	226	deM	C	60s
91.7882	92.0505	413	Kra	C	50s
92.0075	92.3762	823	Ioh	C	15s
92.0661	92.3867	554	Aka	C	60s
92.5366	92.7694	287	deM	C	60s
92.9491	93.3727	1030	Ioh	C	15s
93.3783	93.4599	208	VIR	C	30s
93.5361	93.7695	296	deM	C	60s
93.9749	94.3798	520	Aka	C	60s
94.0172	94.3707	893	Ioh	C	15s
94.1159	94.2477	360	OKU	Rc	30s
94.5085	94.7697	329	deM	C	60s
95.0433	95.3570	404	Aka	C	60s
95.1841	95.3707	477	Ioh	C	15s
95.2823	95.3603	120	Mhh	Ic	50s
95.2828	95.3606	99	Mhh	V	60s
95.5754	95.7112	161	IMi	C	60s
95.9480	96.3715	1000	Ioh	C	15s
95.9731	96.2966	444	OUS	C	60s
96.0769	96.3735	353	Aka	C	60s
96.3357	96.7662	551	deM	C	60s
96.7249	96.8251	125	SWI	C	60s
97.0216	97.3172	711	Ioh	C	15s
97.3349	97.5277	248	deM	C	60s
97.4345	97.7262	849	Rui	C	60s/15s
97.9645	98.2434	588	Ioh	C	15s

*BJD-2455500.

[§]Number of observations.^{||}Observer's code.[#]Filter. "C" means no filter (clear).

Table 4. (Continued.)

Start*	End*	N^{\S}	obs	sys [#]	exp
98.0075	98.3787	454	Aka	C	60s
98.0662	98.2102	197	Mhh	Ic	60s
98.1520	98.3217	129	OKU	V	30s
98.3438	98.7638	513	deM	C	40s/60s
98.3771	98.3876	16	Kai	C	30s
98.7125	98.9376	277	SWI	C	60s
99.0687	99.2541	214	Aka	C	60s
99.1766	99.3704	501	Ioh	C	15s
99.3583	99.7604	661	deM	C	40s
100.0162	100.1296	166	Ioh	C	15s
100.0320	100.3259	357	Aka	C	60s
100.2493	100.3382	209	OKU	Rc	30s
100.3676	100.4750	129	deM	C	60s
100.5620	101.0463	848	Kra	C	40s
101.2780	101.6386	414	Ter	C	60s
101.2909	101.6901	259	Ham	C	120s
101.5025	101.6849	157	deM	C	60s
101.9803	102.1047	299	Siz	C	20s
102.0555	102.1884	335	Ioh	C	15s
102.0806	102.3758	282	Aka	C	60s
102.5646	103.0406	794	Kra	C	40s
103.3178	103.4895	178	deM	C	60s
103.6117	104.0452	726	Kra	C	40s
104.3228	104.5033	228	deM	C	60s
104.5656	105.0448	830	Kra	C	40s
104.5751	104.7502	236	deM	C	60s
104.6818	104.8553	230	SWI	C	60s
105.0303	105.3237	738	Ioh	C	15s
105.0545	105.3793	444	Aka	C	60s
105.0618	105.3481	750	Siz	C	20s
105.6684	105.8555	248	SWI	C	60s
105.6728	105.9557	128	Tze	C	180s
105.7499	106.0439	460	Kra	C	50s
105.8879	106.1951	774	Siz	C	20s
105.9091	106.1330	500	Ioh	C	15s
106.0105	106.1135	140	Mhh	Ic	50s
106.0108	106.1138	140	Mhh	V	50s
106.4233	106.7516	585	deM	C	40s
106.7472	106.9127	209	Kra	C	60s
107.2270	107.3805	195	CRI	C	60s
107.6803	107.8480	220	SWI	C	60s
107.7444	107.8746	206	Kra	C	40s
107.8836	108.1970	841	Siz	C	20s
107.9666	108.3491	417	Aka	C	60s
108.0046	108.1782	442	Ioh	C	15s
108.3286	108.5021	217	deM	C	60s
108.6656	108.8346	222	SWI	C	60s
108.7416	108.8744	210	Kra	C	50s
108.9068	109.1166	194	OKU	C	30s
109.2959	109.5950	129	Ham	C	120s
109.6384	109.8408	263	SWI	C	60s

*BJD–2455500.

[§]Number of observations.^{||}Observer's code.[#]Filter. "C" means no filter (clear).

Table 4. (Continued.)

Start*	End*	N^{\S}	obs	sys [#]	exp
109.7389	109.8747	182	Kra	C	60s
110.3096	110.4380	161	deM	C	60s
110.9516	111.3784	576	Aka	C	60s
111.1731	111.3261	383	Ioh	C	15s
111.6402	111.8384	259	SWI	C	60s
112.6350	112.8428	271	SWI	C	60s
112.9592	113.3599	383	Aka	C	60s
113.3073	113.7121	624	deM	C	60s
113.8963	114.2047	804	Siz	C	20s
113.9407	114.3703	581	Aka	C	60s
114.0164	114.3544	883	Ioh	C	15s
114.3531	114.7079	231	Ham	C	120s
114.3563	114.7528	434	deM	C	60s
114.5701	114.8325	412	Kra	C	50s
114.6531	114.8419	250	SWI	C	60s
114.9430	115.3067	368	Aka	C	60s
115.0414	115.2215	504	OKU	C	30s
115.1288	115.3592	464	Ioh	C	15s
115.3055	115.7433	449	deM	C	60s
115.4450	115.6201	113	Ham	C	120s
115.6005	115.8361	312	SWI	C	60s
115.7667	115.9162	233	Kra	C	50s
116.0311	116.3476	307	Aka	C	60s
116.1918	116.5826	171	CRI	C	180s
116.3069	116.7393	430	deM	C	60s
116.3363	116.4372	166	Vir	C	40s
116.6067	116.8355	303	SWI	C	60s
116.8205	116.9164	142	Kra	C	50s
117.1067	117.2920	497	Ioh	C	15s
117.3084	117.7357	438	deM	C	60s
117.6185	117.6844	46	BBo	C	120s
117.6828	117.9781	371	SWI	C	60s
117.7611	117.9160	243	Kra	C	50s
118.0090	118.3736	491	Aka	C	60s
118.0174	118.3152	721	Ioh	C	15s
118.2117	118.3394	68	CRI	C	150s
118.3091	118.7359	438	deM	C	60s
118.6750	118.9915	402	SWI	C	60s
118.9255	119.0919	404	Ioh	C	15s
119.3099	119.6462	299	deM	C	60s
119.6145	119.6816	46	BBo	C	120s
120.2034	120.3633	581	KU	C	15s
120.3107	120.7317	394	deM	C	60s
120.6472	120.9834	430	SWI	C	60s
121.3146	121.7299	530	deM	C	60s
121.5807	121.6735	60	BBo	C	120s
121.5997	121.8141	283	SWI	C	60s
121.7500	121.9161	257	Kra	C	50s
122.5434	122.6705	179	DPV	V	30s
122.6069	122.7674	100	BBo	C	120s
122.7472	122.9159	267	Kra	C	50s

*BJD−2455500.

[§]Number of observations.^{||}Observer's code.[#]Filter. "C" means no filter (clear).

Table 4. (Continued.)

Start*	End*	N^{\S}	obs	sys [#]	exp
122.7740	122.9897	280	SWI	C	60s
122.9399	123.3472	485	Aka	C	60s
123.3837	123.5611	118	CRI	C	120s
123.3886	123.4930	137	DPV	V	30s
123.5855	123.8297	147	BBo	C	120s
123.6400	123.8103	225	SWI	C	60s
123.7444	123.9162	269	Kra	C	50s
123.9091	123.9275	21	Sac	C	60s
123.9348	124.3598	436	Aka	C	60s
124.0499	124.1438	138	Mhh	Ic	50s
124.0502	124.1441	137	Mhh	V	50s
124.0954	124.1545	171	KU	C	15s
124.2111	124.3360	182	OUS	C	50s
124.2148	124.6109	937	CRI	C	30s
124.2581	124.6708	1101	DPV	C	30s
124.3066	124.4592	362	Kai	C	30s
124.3613	124.7064	224	Ham	C	120s
124.7416	124.9162	277	Kra	C	50s
124.9840	125.1650	290	OUS	C	50s
124.9999	125.3501	936	Ioh	C	15s
125.0662	125.3525	396	Aka	C	60s
125.1928	125.4915	709	CRI	C	30s
125.2698	125.5950	210	Ham	C	120s
125.2941	125.3311	96	Kai	C	30s
125.5703	125.6805	70	BBo	C	120s
125.7389	125.8501	176	Kra	C	50s
125.7667	125.9886	288	SWI	C	60s
125.9322	126.2387	496	Aka	C	60s
125.9501	126.3087	735	Ioh	C	15s
125.9525	126.3509	1036	Siz	C	30s
126.0425	126.1294	140	Mhh	Ic	45s
126.0428	126.1297	140	Mhh	V	45s
126.3339	126.5086	135	Shu	V	20s
126.3343	126.5091	133	Shu	R	20s
126.3351	126.4722	101	Shu	B	20s
126.3568	126.5146	101	Ham	C	120s
126.3832	126.4438	81	CRI	C	60s
126.6707	126.7842	70	BBo	C	120s
126.9105	127.1181	504	Ioh	C	15s
127.2797	127.7019	274	Ham	C	120s
127.3103	127.7107	531	deM	C	40s/60s
127.9194	128.3468	768	Aka	C	60s
128.2648	128.6815	207	Shu	B	160s
128.2652	128.6821	213	Shu	V	160s
128.2656	128.6825	269	Shu	R	120s
128.2683	128.4314	39	Shu	U	180s
128.2702	128.6578	1009	DPV	C	30s
128.2863	128.6989	268	Ham	C	120s
128.2870	128.4372	365	Kai	C	30s
128.4057	128.4337	10	Shu	I	180s
128.7641	128.9829	284	SWI	C	60s

*BJD–2455500.

[§]Number of observations.^{||}Observer's code.[#]Filter. "C" means no filter (clear).

Table 4. (Continued.)

Start*	End*	N^{\S}	obs	sys [#]	exp
128.9004	129.2091	800	Siz	C	30s
128.9373	129.3308	656	Aka	C	60s
129.0103	129.1282	189	Mhh	Ic	45s
129.0106	129.1285	189	Mhh	V	45s
129.0571	129.3483	778	Ioh	C	15s
129.2803	129.5875	197	Ham	C	120s
129.6139	129.9844	475	SWI	C	60s
129.7005	129.8405	90	BBo	C	120s
129.7285	129.9161	293	Kra	C	50s
129.9553	130.3319	513	Aka	C	60s
130.0086	130.3436	842	Ioh	C	15s
130.0463	130.1540	291	Siz	C	30s
130.2247	130.4445	144	Shu	B	20s
130.2252	130.4418	139	Shu	V	20s
130.2256	130.4513	69	Shu	R	40s
130.3610	130.4372	14	Shu	U	90s
130.5846	130.7521	99	BBo	C	120s
130.7257	130.9158	301	Kra	C	50s
130.7466	130.9762	298	SWI	C	60s
130.9167	131.0890	204	Aka	C	60s
131.0232	131.2186	455	Siz	C	30s
131.1061	131.3436	617	Ioh	C	15s
131.6867	131.9162	360	Kra	C	50s
132.0153	132.2564	998	OKU	C	15s
132.0286	132.3419	823	Ioh	C	15s
132.1041	132.3238	304	Aka	C	60s
132.3389	132.3956	34	SAO	V	120s
132.3389	132.6486	104	Shu	V	60s
132.4762	132.5614	41	Shu	U	60s
132.4778	132.6518	73	Shu	R	60s
132.5630	132.6349	55	Shu	B	60s
132.6500	132.6512	2	Shu	I	60s
132.7368	132.9163	285	Kra	C	50s
132.9279	133.1359	279	Aka	C	60s
133.1202	133.2554	280	OKU	C	30s
133.2700	133.6167	312	CRI	C	90s
133.9088	134.3309	1062	Ioh	C	15s
133.9245	134.2841	492	Aka	C	60s
134.1900	134.4818	248	CRI	C	90s
134.2789	134.3441	39	SAO	V	60s
134.2789	134.3441	39	Shu	V	60s
134.4224	134.5509	794	Ter	C	10s
134.7312	134.8743	226	Kra	C	50s
134.7416	134.9449	262	SWI	C	60s
135.1712	135.5455	1348	CRI	C	15s
135.2032	135.6222	371	Ter	C	90s
135.2039	135.3027	268	Ioh	C	15s
135.2756	135.4712	469	Kai	C	30s
135.4246	135.5254	322	VIR	C	20s
136.1744	136.5891	1583	Ter	C	30s
136.1880	136.5348	294	CRI	C	90s

*BJD−2455500.

[§]Number of observations.^{||}Observer's code.[#]Filter. "C" means no filter (clear).

Table 4. (Continued.)

Start*	End*	N^{\S}	obs	sys [#]	exp
136.2261	136.3512	171	Aka	C	60s
136.2817	136.6931	267	Ham	C	120s
136.3263	136.4211	303	VIR	C	20s
136.3305	136.4522	295	deM	C	30s
136.9200	137.3281	528	Aka	C	60s
137.0363	137.3222	748	Ioh	C	15s
137.1971	137.4967	95	CRI	C	30s
137.3264	137.4226	244	VIR	C	30s
137.4029	137.6006	334	deM	C	40s
137.7229	137.8747	240	Kra	C	50s
137.7254	137.8994	226	SWI	C	60s
137.9264	138.3264	960	Siz	C	30s
137.9326	138.3355	1056	Ioh	C	15s
137.9491	138.1159	211	OUS	C	60s
138.0873	138.3314	333	Aka	C	60s
138.1119	138.2418	204	OKU	C	30s
138.3358	138.4769	181	deM	C	40s
138.7122	138.9233	274	SWI	C	60s
138.7201	138.8744	242	Kra	C	50s
139.4819	139.6697	220	deM	C	40s
139.9114	140.2276	836	Siz	C	30s
139.9292	140.1715	264	Aka	C	60s
140.0031	140.2083	488	Ioh	C	15s
140.3493	140.6668	304	deM	C	40s/60s
140.7078	140.9175	272	SWI	C	60s
140.7145	140.8744	251	Kra	C	50s
141.0274	141.2366	481	Ioh	C	15s
141.1954	141.5325	209	CRI	C	120s
141.3484	141.6251	320	deM	C	60s
141.4013	141.5861	55	Shu	R	90s
141.4029	141.5821	39	Shu	V	90s
141.4048	141.5810	37	Shu	B	90s
141.4842	141.4867	2	Shu	I	20s
141.4951	141.5846	15	Shu	U	90s
142.2938	142.6185	212	Ham	C	120s
142.3131	142.5250	80	Shu	WF	90s
142.3206	142.5851	46	Shu	B	90s
142.3220	142.6063	49	Shu	V	90s
142.3230	142.6080	48	Shu	R	90s
142.9223	143.3345	488	Aka	C	60s
142.9728	143.2752	366	OUS	C	60s
143.2329	143.2755	13	Shu	R	90s
143.2344	143.2711	12	Shu	V	90s
143.2667	143.2745	2	Shu	B	90s
143.2798	143.4127	88	CRI	C	120s
143.2931	143.6647	242	Ham	C	120s
143.4544	143.6456	348	deM	C	60s
143.7062	143.8741	264	Kra	C	50s
143.9605	144.0718	151	Mhh	Ic	60s
143.9608	144.0721	151	Mhh	V	60s
143.9658	144.2904	403	Aka	C	60s

*BJD–2455500.

[§]Number of observations.^{||}Observer's code.[#]Filter. "C" means no filter (clear).

Table 4. (Continued.)

Start*	End*	N^{\S}	obs	sys [#]	exp
144.0835	144.2111	331	Siz	C	30s
144.2552	144.6427	875	DPV	C	30s
144.2733	144.5137	72	Shu	R	90s
144.2936	144.6646	242	Ham	C	120s
144.3105	144.4844	44	Shu	V	90s
144.3118	144.4858	45	Shu	B	90s
144.4802	144.6598	350	deM	C	40s
144.7042	144.8743	267	Kra	C	50s
144.9214	145.2836	483	Aka	C	60s
144.9913	145.2504	693	Ioh	C	15s
145.0909	145.2778	254	OUS	C	60s
145.2830	145.5176	99	Shu	R	90s
145.2844	145.5144	67	Shu	V	90s
145.2855	145.4412	30	Shu	U	90s
145.2881	145.5136	65	Shu	B	90s
145.2924	145.4432	7	Shu	I	90s
145.3090	145.6646	229	Ham	C	120s
145.5867	145.9360	649	Kra	C	40s
146.1105	146.2795	121	OUS	C	60s
146.2122	146.6082	273	CRI	C	120s
146.6644	146.9002	308	SWI	C	60s
146.7105	146.8745	254	Kra	C	50s
146.9158	147.2935	455	Aka	C	60s
146.9547	147.2923	897	Ioh	C	15s
147.0929	147.2741	241	OUS	C	60s
147.2127	147.4845	374	CRI	C	60s
147.3700	147.5056	488	Ter	C	15s
147.5863	147.8116	350	Kra	C	50s
147.6696	147.9005	302	SWI	C	60s
147.9645	148.1953	264	Ioh	C	15s
148.0463	148.3163	367	Aka	C	60s
148.3025	148.4106	70	Ham	C	120s
148.3062	148.4736	58	Shu	R	90s
148.3130	148.4724	42	Shu	V	90s
148.3144	148.4341	27	Shu	B	90s
148.3566	148.4379	221	DPV	CR	30s
148.5862	148.8121	355	Kra	C	50s
148.6593	148.9061	316	SWI	C	60s
148.9362	149.1895	342	Aka	C	60s
149.0315	149.1995	667	KU	C	15s
149.1008	149.3003	535	Ioh	C	15s
149.2200	149.5110	130	CRI	C	180s
149.2986	149.6230	209	Ham	C	120s
149.3193	149.4617	217	deM	C	60s
149.3365	149.6012	433	VIR	C	45s
149.5876	149.7499	255	Kra	C	50s
150.2488	150.3154	16	CRI	C	180s
150.2634	150.6256	959	DPV	C	30s
150.2647	150.3412	33	Shu	R	90s
150.2657	150.3402	15	Shu	V	90s
150.2733	150.3424	15	Shu	B	90s

*BJD−2455500.

[§]Number of observations.^{||}Observer's code.[#]Filter. "C" means no filter (clear).

Table 4. (Continued.)

Start*	End*	N^{\S}	obs	sys [#]	exp
150.2973	150.6230	211	Ham	C	120s
150.5371	150.6447	128	deM	C	60s
150.6679	150.7775	143	SWI	C	60s
150.9174	151.2824	485	Aka	C	60s
151.0805	151.2645	253	OUS	C	60s
151.1086	151.2223	453	KU	C	15s
151.3637	151.5775	93	Shu	R	90s
151.3657	151.5782	49	Shu	V	90s
151.3667	151.5792	50	Shu	B	90s
151.3750	151.5476	32	Shu	U	90s
151.4174	151.6269	534	DPV	C	30s
151.4285	151.6036	288	VIR	C	45s
151.5277	151.6413	141	deM	C	60s
151.9442	152.2237	347	Aka	C	60s
151.9501	152.2974	934	Ioh	C	15s
152.0069	152.1995	882	KU	C	15s
152.0836	152.2618	246	OUS	C	60s
152.2624	152.3915	35	Shu	R	90s
152.2634	152.3921	29	Shu	V	90s
152.2656	152.3907	25	Shu	B	90s
152.2728	152.3892	26	Shu	U	90s
152.3846	152.5000	270	DPV	C	30s
152.5003	152.5949	224	DPV	C	30s
152.5377	152.6399	125	deM	C	60s
152.5889	152.7499	253	Kra	C	50s
152.6772	152.9022	292	SWI	C	60s
152.9345	153.2607	442	Aka	C	60s
153.0965	153.2585	428	Ioh	C	15s
153.1051	153.2036	306	KU	C	15s
153.2177	153.4463	107	CRI	C	120s
153.5892	153.7501	250	Kra	C	50s
153.6620	153.9005	312	SWI	C	60s
153.9668	154.0239	73	Aka	C	60s
154.4154	154.6404	87	Shu	C	90s
154.5897	154.7482	249	Kra	C	50s
154.9240	155.2622	461	Aka	C	60s
155.0849	155.2164	603	KU	C	15s
155.0850	155.2605	240	OUS	C	60s
155.2590	155.6399	168	Shu	C	180s
155.2774	155.6197	838	DPV	C	30s
155.2937	155.5186	133	CRI	C	120s
155.9372	156.2702	451	Aka	C	60s
155.9690	156.3022	895	Ioh	C	15s
156.0398	156.2140	793	KU	C	15s
156.4494	156.6226	259	deM	C	50s
156.9365	157.2170	375	Aka	C	60s
156.9765	157.2417	721	Ioh	C	15s
156.9823	157.1990	990	KU	C	15s
157.2723	157.6329	148	Shu	Rc	90s
157.2967	157.5725	364	DPV	C	30s
157.3123	157.3429	51	VIR	C	45s

*BJD–2455500.

[§]Number of observations.^{||}Observer's code.[#]Filter. "C" means no filter (clear).

Table 4. (Continued.)

Start*	End*	N^{\S}	obs	sys [#]	exp
157.4044	157.4497	61	Shu	Ic	20s
157.9871	158.2296	657	Ioh	C	15s
158.0054	158.1344	274	OKU	C	30s
158.3197	158.6230	197	Ham	C	120s
158.5591	158.6887	402	Rui	C	15s
158.9997	159.1483	641	OKU	C	15s
160.2383	160.3212	55	CRI	C	120s
160.3189	160.6231	198	Ham	C	120s
161.3222	161.6231	196	Ham	C	120s
161.9494	162.2409	375	Aka	C	60s
162.3239	162.6230	192	Ham	C	120s
162.5021	162.6128	54	Shu	Rc	90s
162.9359	163.2250	375	Aka	C	60s
163.9436	164.2228	599	OKU	C	30s
163.9660	164.2264	351	Aka	C	60s
163.9750	164.2913	853	Ioh	C	15s
164.3312	164.6231	186	Ham	C	120s
164.9329	164.9825	131	Ioh	C	15s
165.0162	165.2082	743	KU	C	15s
165.0416	165.1812	300	OKU	C	30s
165.0940	165.2227	174	OUS	C	60s
165.1022	165.2505	206	Aka	C	60s
165.2558	165.3583	35	Shu	R	90s
165.2660	165.3550	32	Shu	V	90s
165.3063	165.5346	288	DPV	C	60s
165.3159	165.3567	13	Shu	B	90s
165.3512	165.5214	108	Shu	C	90s
165.3512	165.5214	108	Shu	Rc	90s
165.9782	166.0934	175	Ioh	C	15s
166.0009	166.0775	105	Aka	C	60s
167.3479	167.5160	110	Ham	C	120s
167.4106	167.4995	310	Rui	C	15s
168.0178	168.2906	377	Aka	C	60s
168.0300	168.2075	238	OUS	C	60s
168.2850	168.6185	171	Shu	Rc	90s
168.3369	168.4207	18	Shu	R	90s
168.3381	168.4219	19	Shu	V	90s
168.3395	168.4193	17	Shu	B	90s
169.3892	169.6187	77	Shu	Rc	90s
170.4480	170.6076	72	Shu	Rc	90s
170.9865	171.2319	183	Aka	C	60s
171.3301	171.6231	192	Ham	C	120s
171.9668	172.1662	272	Aka	C	60s
172.0676	172.2049	186	OUS	C	60s
172.0909	172.2196	543	KU	C	15s
172.2245	172.3319	51	CRI	C	120s
172.2860	172.5831	404	DPV	C	30s
172.3290	172.6231	182	Ham	C	120s
172.4002	172.4486	65	IMi	C	60s
173.0345	173.1216	214	KU	C	15s
173.2521	173.4699	143	CRI	C	120s

*BJD−2455500.

[§]Number of observations.^{||}Observer's code.[#]Filter. "C" means no filter (clear).

Table 4. (Continued.)

Start*	End*	N^{\S}	obs	sys [#]	exp
173.2855	173.6153	237	Shu	Rc	30s
173.2861	173.3729	22	Shu	B	90s
173.2866	173.3738	18	Shu	V	90s
173.2881	173.3752	19	Shu	U	90s
173.3691	173.5789	274	IMi	V	60s
174.2897	174.3630	98	DPV	C	30s
174.2927	174.3869	35	Shu	B	90s
174.2939	174.3852	34	Shu	U	90s
174.2951	174.5946	417	Shu	Rc	20s
174.2974	174.3864	34	Shu	V	90s
174.2978	174.3873	15	Shu	Ic	90s
175.0449	175.2423	270	Aka	C	60s
175.2126	175.2799	253	KU	C	15s
175.9957	176.2547	343	Aka	C	60s
176.0491	176.1949	565	KU	C	15s
176.0719	176.2121	371	Ioh	C	15s
176.3037	176.4764	226	CRI	C	60s
176.9412	177.1276	478	Siz	C	30s
177.0146	177.2097	564	KU	C	15s
177.3023	177.4898	248	DPV	C	30s
177.9824	178.2447	354	Aka	C	60s
178.2781	178.3799	135	CRI	C	60s
178.2950	178.3388	30	Shu	C	30s
178.3756	178.5548	201	deM	C	50s
178.4010	178.5131	184	VIR	C	45s
179.2933	179.4487	71	CRI	C	180s
179.3625	179.5553	240	deM	C	50s
180.0578	180.2164	195	Aka	C	60s
180.2321	180.3111	366	KU	C	15s
180.3077	180.5079	92	CRI	C	180s
181.0041	181.1988	711	KU	C	15s
181.0509	181.1820	358	Ioh	C	15s
182.3018	182.5007	133	CRI	C	120s
182.3985	182.5936	165	Ham	C	90s
182.4023	182.4603	79	IMi	V	60s
183.0322	183.1542	294	Ioh	C	15s
183.1535	183.1918	120	KU	C	15s
183.3500	183.6056	312	Ham	C	60s
183.9424	184.1185	223	Aka	C	60s
183.9892	184.1896	249	KU	C	15s
184.2969	184.4258	131	DPV	C	30s
184.3007	184.4606	117	CRI	C	110s
184.3566	184.6071	305	Ham	C	60s
185.3574	185.6050	300	Ham	C	60s
185.3850	185.5023	54	CRI	C	180s
186.3510	186.6053	307	Ham	C	60s
186.9646	187.2131	339	Aka	C	60s
186.9663	187.1825	941	KU	C	15s
187.3066	187.5859	221	Shu	C	60s
187.3450	187.6042	225	Ham	C	90s
188.2825	188.5714	190	Shu	C	90s

*BJD–2455500.

[§]Number of observations.^{||}Observer's code.[#]Filter. "C" means no filter (clear).

Table 4. (Continued.)

Start*	End*	N^{\S}	obs	sys [#]	exp
188.2893	188.4902	133	CRI	C	90s
188.3728	188.6033	168	Ham	C	100s
189.0673	189.2310	422	Ioh	C	15s
189.2754	189.4815	141	CRI	C	120s
189.9888	190.1950	274	Aka	C	60s
190.0895	190.1488	75	KU	C	15s
190.2917	190.5815	198	Shu	C	90s
190.3822	190.5574	539	Rui	C	15s
190.4082	190.5689	209	IMi	C	60s
191.3340	191.5771	112	Shu	C	90s
192.2719	192.4692	106	CRI	C	150s
193.3115	193.5542	322	DPV	C	30s
194.3905	194.6037	182	Ham	C	90s
194.9459	195.1434	273	Aka	C	60s
195.9465	196.1729	307	Aka	C	60s
197.2622	197.4690	97	CRI	C	180s
198.2712	198.4347	77	CRI	C	180s
199.0537	199.1781	169	Aka	C	60s
199.2778	199.4153	63	CRI	C	180s
199.9491	200.1868	325	Aka	C	60s
200.0005	200.1284	498	KU	C	15s
200.2561	200.4086	72	CRI	C	180s
200.3151	200.5465	295	DPV	C	30s
200.9485	201.1505	278	Aka	C	60s
201.0919	201.1445	182	KU	C	15s
201.2603	201.4184	73	CRI	C	180s
201.9539	202.0385	84	Aka	C	60s
202.0082	202.1413	381	KU	C	15s
202.3795	202.5834	174	Ham	C	90s
203.3797	203.4749	73	Ham	C	90s
204.3833	204.5628	152	Ham	C	90s
205.2796	205.4469	73	CRI	C	180s
205.9838	206.1055	100	Aka	C	60s
206.2906	206.4196	60	CRI	C	180s
207.2783	207.4128	63	CRI	C	180s
207.3619	207.5292	179	NKa	C	70s
208.2654	208.3942	50	CRI	C	180s
209.2673	209.3585	43	CRI	C	180s
210.2773	210.3011	9	CRI	C	180s
211.3259	211.5250	246	DPV	C	30s
211.3848	211.5817	169	Ham	C	90s
212.3393	212.5117	238	DPV	C	30s
212.3873	212.4283	20	CRI	C	180s
213.2956	213.3106	8	CRI	C	150s
214.2643	214.3814	55	CRI	C	180s
214.3811	214.5731	165	Ham	C	90s
215.0263	215.1139	113	Aka	C	60s
216.9723	217.0540	109	Aka	C	60s
218.0176	218.1189	137	Aka	C	60s
218.2988	218.3742	36	CRI	C	180s
219.2860	219.3598	35	CRI	C	180s

*BJD−2455500.

[§]Number of observations.^{||}Observer's code.[#]Filter. "C" means no filter (clear).

Table 4. (Continued.)

Start*	End*	N^{\S}	obs	sys [#]	exp
220.2784	220.3522	35	CRI	C	180s
220.3614	220.3780	47	DPV	C	30s
221.2729	221.3488	36	CRI	C	180s
222.2933	222.4011	47	CRI	C	180s
233.9745	234.0597	119	Aka	C	60s
240.9856	241.0651	105	Aka	C	60s
252.9643	253.0706	145	Aka	C	60s
253.9688	254.0852	150	Aka	C	60s
255.0095	255.0776	93	Aka	C	60s
257.9896	258.0612	93	Aka	C	60s
258.9653	259.0434	109	Aka	C	60s
262.9793	263.0475	70	Aka	C	60s
400.6318	400.7674	170	deM	C	60s
401.6245	401.7610	177	deM	C	60s
402.5931	402.7667	224	deM	C	60s
405.1334	405.2534	187	OKU	C	30s
405.2411	405.3437	398	KU	C	15s
406.1739	406.2584	137	OKU	C	30s
407.2635	407.3860	274	OKU	C	30s
410.2192	410.3276	384	KU	C	15s
410.5449	410.7707	291	deM	C	60s
411.2529	411.3409	265	KU	C	15s
412.1101	412.2632	420	OKU	C	30s
412.1450	412.3155	240	OUS	C	60s
412.2951	412.3847	410	KU	C	15s
413.1334	413.3133	251	OUS	C	60s
413.1844	413.2627	168	OKU	C	30s
414.5778	414.7722	259	deM	C	50s
415.5750	415.7719	264	deM	C	50s
416.5745	416.7721	264	deM	C	50s
417.5298	417.7721	323	deM	C	50s
418.5337	418.7723	318	deM	C	50s
419.5141	419.7658	335	deM	C	50s
420.1247	420.2652	392	OKU	C	20s
420.3159	420.3691	126	Mhh	C	30s
421.1969	421.3432	485	OKU	C	20s
421.4615	421.7712	372	deM	C	60s
422.2400	422.3598	427	KU	C	15s
422.5797	422.7709	243	deM	C	60s
423.5737	423.7441	220	deM	C	60s
424.4237	424.5677	68	CRI	C	180s
425.3279	425.3623	17	CRI	C	180s
425.6594	425.7673	142	deM	C	60s
427.2441	427.3234	99	OKU	C	60s
429.4212	429.7636	507	deM	C	50s
430.2972	430.3898	111	Aka	C	60s
430.4310	430.7641	498	deM	C	50s
431.0769	431.3908	327	Aka	C	60s
431.2887	431.3262	187	OKU	C	10s
431.4491	431.7639	473	deM	C	50s
432.0758	432.3870	421	Aka	C	60s

*BJD–2455500.

[§]Number of observations.^{||}Observer’s code.[#]Filter. “C” means no filter (clear).

Table 4. (Continued.)

Start*	End*	N^{\S}	obs	sys [#]	exp
432.1526	432.2814	427	OKU	C	20s
432.4491	432.7222	393	deM	C	50s
432.7184	432.9505	549	SWI	C	30s
433.0257	433.1746	205	Aka	C	60s
433.1181	433.1680	94	OKU	C	30s
433.4813	433.7120	345	deM	C	50s
433.7205	433.9592	568	SWI	C	30s
434.1071	434.1765	177	OKU	C	30s
434.1626	434.3934	319	Aka	C	60s
434.5138	434.7672	372	deM	C	50s
435.5183	435.7497	347	deM	C	50s
436.1334	436.3947	673	OKU	C	30s
436.1764	436.3933	297	Aka	C	60s
437.4966	437.7652	401	deM	C	50s
437.7663	438.0500	641	Ham	C	30s
438.1536	438.3321	464	OKU	C	30s
438.1763	438.3509	164	Aka	C	90s
438.5217	438.7653	362	deM	C	50s
439.6275	439.7226	146	deM	C	50s
440.6808	441.0009	754	Ham	C	30s
443.5130	443.7650	382	deM	C	50s
444.0133	444.2663	326	OKU	C	60s
444.2022	444.3335	630	KU	C	15s
444.5645	444.7650	302	deM	C	50s
444.6546	444.7029	108	Ham	C	30s
444.7109	444.9329	291	SWI	C	60s
445.0188	445.0727	73	OKU	C	60s
445.7030	445.9290	293	SWI	C	60s
445.8825	446.0523	397	Ham	C	30s
446.2813	446.5418	115	CRI	C	180s
446.6058	446.7651	246	deM	C	50s
446.6962	446.9253	554	SWI	C	30s
446.8826	447.0524	400	Ham	C	30s
447.6844	447.9262	585	SWI	C	30s
447.8823	448.0522	400	Ham	C	30s
448.6161	448.7668	233	deM	C	50s
450.6018	450.7427	216	deM	C	50s
452.0434	452.2581	229	OKU	C	70s
452.6021	452.7675	175	deM	C	70s
452.6796	452.9170	570	SWI	C	30s
452.6944	452.8503	370	Ham	C	30s
453.1151	453.2357	166	OUS	C	60s
453.1175	453.2499	271	OKU	C	30s
453.8633	454.0501	440	Ham	C	30s
454.2662	454.5835	139	CRI	C	180s
454.6019	454.7676	256	deM	C	50s
455.2159	455.3197	142	Aka	C	60s
455.2260	455.6258	178	CRI	C	180s
455.7169	455.9063	456	SWI	C	30s
455.8659	456.0524	437	Ham	C	30s
456.6160	456.7662	232	deM	C	50s

*BJD−2455500.

[§]Number of observations.^{||}Observer's code.[#]Filter. "C" means no filter (clear).

Table 4. (Continued.)

Start*	End*	N^{\S}	obs	sys [#]	exp
456.6642	456.8992	568	SWI	C	30s
457.1511	457.3774	210	Aka	C	90s
457.4431	457.7029	632	DPV	C	30s
457.7519	457.8948	348	DPV	C	30s
457.8437	460.0401	2156	Ham	C	80s
458.0906	458.2346	192	Aka	C	60s
458.4367	458.6848	630	DPV	C	30s
459.1133	459.3638	329	Aka	C	30s
459.4343	459.7012	643	DPV	C	30s
459.7330	459.8952	395	SWI	C	30s
460.1322	460.3618	309	Aka	C	60s
460.4348	460.7003	290	DPV	C	30s
460.6249	460.7658	213	deM	C	50s
460.6403	460.8504	502	SWI	C	30s
460.8967	461.0397	329	Ham	C	30s
461.2501	461.3572	90	Aka	C	90s
462.2115	462.3781	230	Aka	C	60s
462.2386	462.6140	166	CRI	C	180s
463.2313	463.4606	96	CRI	C	180s
463.6202	463.8805	628	SWI	C	30s
463.7050	463.9222	509	Ham	C	30s
464.2403	464.3568	50	CRI	C	180s
464.2898	464.7282	132	Ham	C	120s
465.1728	465.3753	184	Aka	C	90s
466.2170	466.3745	148	Aka	C	90s
466.2457	466.7264	147	Ham	C	120s
466.6072	466.8666	616	SWI	C	30s
467.2329	467.3667	115	Aka	C	90s
467.2831	467.5094	103	CRI	C	180s
467.6049	467.8667	620	SWI	C	30s
468.2095	468.3831	163	Aka	C	90s
468.2364	468.3052	33	CRI	C	180s
468.2570	468.7270	120	Ham	C	120s
468.6957	468.8701	414	CRI	C	30s
469.1586	469.3729	201	Aka	C	90s
469.2565	469.3371	53	Ham	C	120s
470.2396	470.4597	568	DPV	C	30s
471.2298	471.4295	519	DPV	C	30s
471.2369	471.3917	73	CRI	C	180s
471.5972	471.7469	329	Ham	C	30s
471.6105	471.8651	615	SWI	C	30s
472.2240	472.2862	160	DPV	C	30s
473.6029	473.8572	618	SWI	C	30s
473.8614	473.9463	40	APO	R	180s
473.8754	474.0234	445	AKz	C	30s
475.1651	475.3750	197	Aka	C	90s
476.1801	476.3762	184	Aka	C	90s
476.6262	476.7501	192	deM	C	50s
476.8672	477.0150	329	Ham	C	30s
477.1710	477.3746	189	Aka	C	90s
477.3819	477.7083	159	Ham	C	120s

*BJD–2455500.

[§]Number of observations.^{||}Observer’s code.[#]Filter. “C” means no filter (clear).

Table 4. (Continued.)

Start*	End*	N^{\S}	obs	sys [#]	exp
477.6162	477.7497	196	deM	C	50s
478.1433	478.3747	186	Aka	C	90s
478.2981	478.5067	135	CRI	C	120s
478.3459	478.6813	801	DPV	C	30s
478.6127	478.8440	563	SWI	C	30s
478.6163	478.7547	261	deM	C	40s
478.8616	479.0093	363	Ham	C	30s
479.3933	479.4937	61	Ham	C	30s
479.5935	479.7534	296	deM	C	40s
479.8589	480.0067	358	Ham	C	30s
480.5946	480.7275	180	deM	C	60s
480.8561	481.0039	359	Ham	C	30s
481.1812	481.4418	159	CRI	C	120s
481.8533	482.0011	358	Ham	C	30s
481.8559	481.9245	45	APO	R	90s
482.3181	482.7385	746	deM	C	40s
482.8505	482.9983	359	AKz	C	30s
482.8516	482.9193	40	APO	R	90s
483.8306	483.9266	60	APO	R	90s
483.8478	483.9956	358	AST	C	30s
484.0031	484.2401	340	OKU	C	50s
484.1190	484.3624	326	Aka	C	30s
484.3170	484.7377	754	deM	C	40s
484.8433	484.9371	39	APO	R	90s
484.8450	484.9424	234	AKz	C	30s
484.9443	485.0886	498	OKU	C	20s
485.1385	485.3630	311	Aka	C	60s
485.3151	485.7127	723	deM	C	40s
485.5883	485.7823	326	LCO	B	40s
485.7142	485.9849	638	SWI	C	30s
486.3223	486.7257	690	deM	C	40s
486.7090	486.9844	646	SWI	C	30s
486.8394	486.9869	358	AKz	C	30s
487.1144	487.2779	226	Aka	C	60s
487.2788	487.3998	308	Kai	C	30s
487.3567	487.7180	647	deM	C	40s
487.8366	487.9848	145	AKz	C	30s
487.8438	487.9105	44	APO	R	90s
488.2550	488.4635	524	Kai	C	30s
489.3212	489.7185	725	deM	C	40s
489.8252	489.9030	40	APO	R	90s
489.8311	489.9792	145	AKz	C	30s
490.3179	490.7164	729	deM	C	40s
490.6968	491.0050	695	SWI	C	30s
490.8283	490.9042	50	APO	R	30s
490.8283	490.9769	145	AKz	C	30s
491.2290	491.4005	415	DPV	C	30s
491.7300	491.9911	608	SWI	C	30s
491.8255	491.9736	144	AKz	C	30s
491.8302	491.9222	60	APO	R	90s
492.2372	492.3971	418	DPV	C	30s

*BJD−2455500.

[§]Number of observations.^{||}Observer's code.[#]Filter. "C" means no filter (clear).

Table 4. (Continued.)

Start*	End*	N^{\S}	obs	sys [#]	exp
492.4199	492.7014	521	deM	C	40s
493.4081	493.6106	259	Vir	C	60s
493.4247	493.6060	336	deM	C	40s
494.3928	494.7048	404	NDJ	C	30s
494.4064	494.6458	440	deM	C	40s
495.2855	495.4244	44	Ham	C	120s
495.4157	495.6274	392	deM	C	40s
496.3625	496.4006	100	CRI	C	30s
497.0856	497.3040	205	Aka	C	90s
497.0982	497.2520	200	OKU	C	60s
497.2990	497.3700	200	CRI	C	30s
497.6945	497.9609	630	SWI	C	30s
498.0884	498.3092	207	Aka	C	90s
498.5969	498.9545	347	AKz	C	30s
499.0839	499.3206	326	Aka	C	60s
499.3198	499.5987	394	deM	C	50s
499.3388	499.4757	40	Ham	C	120s
499.7511	499.8799	40	PSD	V	120s
499.9199	500.1075	449	OKU	C	30s
500.0322	500.1840	233	OUS	C	50s
500.1331	500.3276	268	Aka	C	60s
500.3244	500.5589	347	deM	C	50s
500.8087	500.8656	20	PSD	V	30s
501.1033	501.2522	140	Aka	C	90s
501.2746	501.4435	434	Kai	C	30s
501.2863	501.6939	125	Ham	C	120s
501.3128	501.4528	208	deM	C	50s
501.6869	501.9574	640	SWI	C	30s
502.1009	502.2563	66	Aka	C	90s
502.2646	502.4477	469	Kai	C	30s
502.3016	502.6906	118	Ham	C	120s
503.2504	503.5956	447	DPV	C	30s
503.2673	503.4509	476	Kai	C	30s
503.3325	503.4466	33	Ham	C	120s
503.8009	503.8698	45	APO	R	120s
504.2151	504.2519	18	CRI	C	180s
504.2594	504.6283	492	DPV	C	30s
504.2781	504.3504	187	Kai	C	30s
504.3165	504.4709	229	deM	C	50s
504.4208	504.5776	106	Pol	V	60s
504.8086	504.8406	10	PSD	C	120s
505.2564	505.6423	512	DPV	C	30s
505.3086	505.4327	35	Ham	C	120s
505.3151	505.4790	232	deM	C	50s
506.2276	506.5491	148	CRI	C	180s
506.2974	506.6841	117	Ham	C	120s
506.3128	506.4788	247	deM	C	50s
507.0530	507.3031	232	Aka	C	90s
507.2217	507.6148	181	CRI	C	180s
507.2425	507.4697	304	DPV	C	30s
507.2747	507.4275	395	Kai	C	30s

*BJD–2455500.

[§]Number of observations.^{||}Observer's code.[#]Filter. "C" means no filter (clear).

Table 4. (Continued.)

Start*	End*	N^{\S}	obs	sys [#]	exp
508.0741	508.2984	204	Aka	C	90s
508.3443	508.6279	423	deM	C	50s
508.6670	508.9697	725	SWI	C	30s
508.7893	508.8575	45	APO	R	120s
509.2404	509.6015	475	DPV	C	30s
509.2740	509.4287	400	Kai	C	30s
509.2960	509.4775	120	Ham	C	120s
509.3142	509.6609	486	deM	C	50s
509.3807	509.4024	27	Vir	C	30s
509.6621	509.9606	712	SWI	C	30s
510.2730	510.6325	442	DPV	C	30s
510.2974	510.4779	118	Ham	C	120s
510.7116	510.9636	600	SWI	C	30s
511.2568	511.6364	492	DPV	C	30s
511.2986	511.4780	116	Ham	C	120s
511.3313	511.6014	215	CRI	C	100s
511.6616	511.9714	677	SWI	C	30s
511.7843	511.8526	45	APO	R	120s
512.1064	512.1975	86	Aka	C	90s
512.3448	512.5341	142	CRI	C	100s
512.4610	512.6455	284	deM	C	50s
513.3008	513.4357	89	Ham	C	120s
513.3464	513.5437	295	deM	C	50s
513.6533	513.9256	650	SWI	C	30s
514.0302	514.2753	230	Aka	C	90s
514.3210	514.6426	509	deM	C	50s
514.6667	514.9506	678	SWI	C	30s
515.0450	515.2708	212	Aka	C	90s
515.3041	515.4358	87	Ham	C	120s
515.3188	515.5408	326	deM	C	50s
515.6622	515.9495	680	SWI	C	30s
516.6583	516.9533	697	SWI	C	30s
518.6527	518.9470	695	SWI	C	30s
519.0029	519.1708	230	OKU	C	60s
519.0214	519.2667	230	Aka	C	90s
519.2799	519.4124	350	Kai	C	30s
519.3333	519.5502	275	Vir	C	60s
519.6225	519.8238	128	APO	R	120s
519.9808	520.0929	150	OKU	C	60s
520.2885	520.3818	164	Kai	C	30s
520.3317	520.5676	300	Vir	C	60s
521.0101	521.2758	242	Aka	C	90s
521.3434	521.4133	90	Vir	C	60s
521.6488	521.9501	706	SWI	C	30s
521.9281	522.0740	188	OKU	C	60s
522.2675	522.5786	274	CRI	C	90s
522.6423	522.8950	590	SWI	C	30s
523.0150	523.1533	190	Aka	C	60s
523.2013	523.4273	342	CRI	C	50s
524.2836	524.4310	389	Kai	C	30s
525.0338	525.2298	183	Aka	C	90s

*BJD−2455500.

[§]Number of observations.^{||}Observer's code.[#]Filter. "C" means no filter (clear).

Table 4. (Continued.)

Start*	End*	N^{\S}	obs	sys [#]	exp
525.1277	525.2002	100	OKU	C	60s
525.3529	525.6127	394	deM	C	50s
525.7207	525.9603	518	SWI	C	30s
526.1167	526.2295	142	OKU	C	60s
526.3328	526.6065	417	deM	C	50s
526.3806	526.4500	190	Kai	C	30s
527.2792	527.4898	274	DPV	C	60s
527.6442	527.9110	623	SWI	C	30s
528.2642	528.5209	348	DPV	C	60s
529.6486	529.7859	80	APO	R	140s
529.9942	530.1486	122	Aka	C	90s
530.3289	530.5774	365	deM	C	50s
531.3075	531.3456	18	CRI	C	180s
531.6870	531.9181	552	SWI	C	30s
532.0508	532.1893	190	OKU	C	50s
532.3580	532.5960	355	deM	C	50s
532.9351	533.1373	260	Aka	C	60s
533.0956	533.2099	157	OKU	C	60s
533.2494	533.5481	406	CRI	C	60s
533.3296	533.5460	311	deM	C	50s
533.6436	533.9217	664	SWI	C	30s
533.9785	534.2081	314	Aka	C	60s
533.9785	534.2092	427	OUS	C	45s
534.2506	534.4643	295	CRI	C	60s
534.3341	534.5567	338	deM	C	50s
534.3360	534.5821	153	Ham	C	120s
534.6287	534.9207	697	SWI	C	30s
535.0386	535.2630	260	Aka	C	60s
535.0462	535.1690	449	OKU	C	15s
535.3321	535.5365	308	deM	C	50s
535.5784	535.6781	215	LCO	B	30s
535.6222	535.9074	681	SWI	C	30s
536.0508	536.1191	231	OKU	C	15s
536.6184	536.8982	668	SWI	C	30s
536.6505	536.8338	108	APO	R	120s
537.3684	537.5250	200	Vir	C	60s
538.3083	538.3851	206	Kai	C	30s
538.4307	538.5733	220	deM	C	50s
538.6251	538.9015	660	SWI	C	30s
539.3493	539.5169	258	deM	C	50s
540.2750	540.5251	345	CRI	C	60s
540.3359	540.5327	298	deM	C	50s
540.9447	541.2095	361	Aka	C	60s
541.0791	541.1865	252	OKU	C	30s
541.3390	541.5364	303	deM	C	50s
541.9404	542.0951	209	Aka	C	60s
542.3367	542.5314	295	deM	C	50s
542.6230	542.8038	432	SWI	C	30s
543.9660	544.2697	387	Aka	C	60s
544.9395	545.1760	319	Aka	C	60s
546.3242	546.5635	315	DPV	C	30s

*BJD–2455500.

[§]Number of observations.^{||}Observer's code.[#]Filter. "C" means no filter (clear).

Table 4. (Continued.)

Start*	End*	N^{\S}	obs	sys [#]	exp
551.0375	551.1909	199	Aka	C	60s
551.9365	552.1531	197	Aka	C	90s
553.2850	553.4517	468	CRI	C	20s
553.9543	554.1409	171	Aka	C	90s
554.3447	554.5049	450	CRI	C	20s
555.0010	555.1184	110	Aka	C	90s
556.9497	557.1381	173	Aka	C	90s
557.3725	557.5216	230	deM	C	50s
557.9524	558.1406	145	Aka	C	90s
559.0003	559.1310	122	Aka	C	90s
559.9481	560.1253	165	Aka	C	90s
563.9978	564.1136	156	Aka	C	60s
569.3144	569.3755	74	Vol	Rc	60s
570.0090	570.1217	104	Aka	C	90s
570.9599	571.1088	137	Aka	C	90s
574.0236	574.1456	101	Aka	C	90s
574.9683	575.1525	172	Aka	C	90s
575.9570	576.0648	97	Aka	C	90s
576.9617	577.1256	137	Aka	C	90s
577.6484	577.7664	281	SWI	C	30s
581.9754	582.1114	181	Aka	C	60s
588.9636	589.1050	196	Aka	C	60s
590.6471	590.7641	280	SWI	C	30s
591.9666	592.1211	214	Aka	C	60s

*BJD−2455500.

[§]Number of observations.^{||}Observer’s code.[#]Filter. “C” means no filter (clear).

Table 5. Log of the maximum timings of negative superhumps supercycle 2011 S1

E	The timings of maximum*	$O - C$	error
0	91.0210	0.0010	0.0010
1	91.0857	0.0034	0.0014
2	91.1366	-0.0081	0.0010
3	91.2149	0.0079	0.0004
4	91.2706	0.0012	0.0003
5	91.3319	0.0002	0.0003
8	91.5213	0.0026	0.0006
9	91.5830	0.0020	0.0003
10	91.6479	0.0045	0.0004
11	91.7092	0.0035	0.0005
13	91.8352	0.0048	0.0004
14	91.8990	0.0063	0.0005
15	91.9561	0.0010	0.0003
16	92.0147	-0.0028	0.0011
17	92.0853	0.0055	0.0009
18	92.1492	0.0071	0.0006
19	92.2114	0.0069	0.0007
26	92.6447	0.0039	0.0009
27	92.7049	0.0017	0.0006
31	92.9549	0.0024	0.0025
32	93.0163	0.0015	0.0007
33	93.0815	0.0043	0.0010
34	93.1446	0.0051	0.0005
35	93.2025	0.0006	0.0007
36	93.2664	0.0022	0.0006
37	93.3282	0.0016	0.0006
38	93.3887	-0.0002	0.0003
39	93.4558	0.0045	0.0003
41	93.5811	0.0051	0.0004
42	93.6439	0.0056	0.0004
43	93.7080	0.0074	0.0006
44	93.7701	0.0071	0.0005
48	94.0174	0.0051	0.0009
49	94.0838	0.0092	0.0004
50	94.1466	0.0096	0.0002
51	94.2089	0.0096	0.0003
52	94.2645	0.0028	0.0003
53	94.3308	0.0068	0.0005
56	94.5217	0.0106	0.0007
57	94.5786	0.0052	0.0004
58	94.6466	0.0109	0.0005
59	94.7129	0.0148	0.0017
65	95.0800	0.0079	0.0006
66	95.1399	0.0055	0.0006
67	95.2012	0.0044	0.0005
68	95.2673	0.0082	0.0004
69	95.3294	0.0079	0.0008
73	95.5839	0.0131	0.0011
74	95.6443	0.0111	0.0003
75	95.7037	0.0082	0.0005
80	96.0138	0.0066	0.0009
81	96.0797	0.0101	0.0005
82	96.1415	0.0096	0.0012
83	96.2059	0.0117	0.0005
84	96.2665	0.0099	0.0004
*BJD-2455600			

Table 5. (Continued.)

E	The timings of maximum*	$O - C$	error
85	96.3263	0.0074	0.0008
86	96.3907	0.0094	0.0007
87	96.4507	0.0071	0.0003
88	96.5141	0.0082	0.0013
89	96.5767	0.0084	0.0004
90	96.6424	0.0118	0.0003
92	96.7647	0.0094	0.0005
97	97.0762	0.0092	0.0008
98	97.1412	0.0119	0.0008
99	97.2086	0.0169	0.0015
100	97.2631	0.0091	0.0006
101	97.3310	0.0146	0.0012
102	97.3904	0.0117	0.0011
103	97.4557	0.0146	0.0005
104	97.5151	0.0118	0.0003
105	97.5805	0.0148	0.0004
106	97.6441	0.0161	0.0005
107	97.6968	0.0064	0.0004
112	98.0188	0.0167	0.0024
113	98.0816	0.0172	0.0013
114	98.1413	0.0145	0.0007
115	98.2044	0.0153	0.0008
116	98.2669	0.0154	0.0005
117	98.3234	0.0096	0.0003
118	98.3977	0.0216	0.0014
119	98.4545	0.0161	0.0011
120	98.5081	0.0073	0.0010
121	98.5759	0.0127	0.0008
122	98.6327	0.0073	0.0003
123	98.6976	0.0098	0.0011
124	98.7624	0.0122	0.0081
125	98.8246	0.0121	0.0007
126	98.8850	0.0101	0.0011
130	99.1398	0.0156	0.0008
131	99.1883	0.0018	0.0085
133	99.3225	0.0113	0.0030
134	99.3823	0.0088	0.0014
135	99.4515	0.0156	0.0006
136	99.5140	0.0158	0.0004
137	99.5756	0.0151	0.0005
138	99.6382	0.0153	0.0003
139	99.7031	0.0179	0.0005
145	100.0738	0.0145	0.0012
146	100.1355	0.0138	0.0012
147	100.2015	0.0175	0.0005
148	100.2652	0.0189	0.0004
149	100.3243	0.0156	0.0007
150	100.3838	0.0128	0.0011
151	100.4450	0.0117	0.0005
154	100.6386	0.0182	0.0003
155	100.6965	0.0138	0.0005
156	100.7617	0.0167	0.0007
157	100.8236	0.0162	0.0009
158	100.8832	0.0135	0.0008
159	100.9479	0.0159	0.0002
*BJD-2455600			

Table 5. (Continued.)

E	The timings of maximum*	$O - C$	error
160	101.0072	0.0128	0.0003
165	101.3212	0.0151	0.0005
166	101.3789	0.0105	0.0004
167	101.4425	0.0117	0.0013
168	101.5147	0.0216	0.0007
169	101.5705	0.0151	0.0002
170	101.6316	0.0139	0.0002
176	102.0040	0.0121	0.0012
177	102.0636	0.0094	0.0011
178	102.1317	0.0152	0.0005
179	102.1937	0.0149	0.0007
181	102.3143	0.0107	0.0005
182	102.3787	0.0128	0.0002
186	102.6321	0.0168	0.0005
187	102.6930	0.0154	0.0003
188	102.7587	0.0188	0.0006
189	102.8188	0.0166	0.0007
190	102.8770	0.0125	0.0006
191	102.9407	0.0138	0.0003
192	103.0038	0.0145	0.0008
198	103.3778	0.0145	0.0012
199	103.4415	0.0158	0.0022
202	103.6263	0.0136	0.0011
203	103.6883	0.0133	0.0003
204	103.7560	0.0186	0.0008
206	103.8776	0.0156	0.0007
207	103.9370	0.0126	0.0006
208	104.0043	0.0176	0.0009
214	104.3729	0.0121	0.0009
215	104.4386	0.0155	0.0005
216	104.5010	0.0155	0.0005
218	104.6293	0.0192	0.0006
219	104.6846	0.0121	0.0004
220	104.7535	0.0187	0.0006
221	104.8090	0.0119	0.0004
222	104.8762	0.0167	0.0002
223	104.9395	0.0177	0.0009
224	104.9994	0.0152	0.0002
225	105.0629	0.0164	0.0005
226	105.1244	0.0155	0.0004
227	105.1875	0.0164	0.0003
228	105.2468	0.0133	0.0008
229	105.3077	0.0119	0.0010
230	105.3742	0.0160	0.0003
235	105.6906	0.0207	0.0006
236	105.7487	0.0165	0.0005
237	105.8112	0.0167	0.0006
238	105.8663	0.0094	0.0006
239	105.9344	0.0152	0.0015
240	106.0046	0.0231	0.0009
241	106.0580	0.0140	0.0011
242	106.1221	0.0158	0.0008
243	106.1854	0.0168	0.0019
248	106.4954	0.0151	0.0005
250	106.6221	0.0171	0.0003
*BJD-2455600			

Table 5. (Continued.)

E	The timings of maximum*	$O - C$	error
251	106.6792	0.0119	0.0004
252	106.7460	0.0163	0.0004
253	106.8057	0.0137	0.0011
254	106.8708	0.0164	0.0013
261	107.3024	0.0116	0.0007
262	107.3662	0.0131	0.0006
268	107.7360	0.0088	0.0010
269	107.8029	0.0134	0.0004
270	107.8591	0.0073	0.0005
272	107.9807	0.0042	0.0008
273	108.0522	0.0134	0.0008
274	108.1067	0.0056	0.0005
275	108.1797	0.0162	0.0003
276	108.2419	0.0161	0.0012
278	108.3574	0.0069	0.0004
279	108.4284	0.0155	0.0009
284	108.7351	0.0105	0.0007
285	108.7976	0.0107	0.0004
286	108.8617	0.0124	0.0002
287	108.9258	0.0142	0.0009
288	108.9900	0.0161	0.0004
300	109.7315	0.0095	0.0021
301	109.7956	0.0112	0.0008
302	109.8582	0.0116	0.0008
310	110.3521	0.0067	0.0009
311	110.4163	0.0085	0.0006
320	110.9740	0.0052	0.0011
321	111.0405	0.0093	0.0007
322	111.1021	0.0086	0.0011
323	111.1697	0.0139	0.0009
324	111.2291	0.0110	0.0009
325	111.2820	0.0015	0.0006
326	111.3529	0.0100	0.0007
331	111.6634	0.0089	0.0004
332	111.7235	0.0066	0.0006
347	112.6572	0.0053	0.0008
348	112.7221	0.0078	0.0007
349	112.7834	0.0067	0.0004
353	113.0335	0.0074	0.0008
354	113.0937	0.0054	0.0004
356	113.2221	0.0091	0.0008
357	113.2797	0.0044	0.0007
358	113.3427	0.0050	0.0007
359	113.4082	0.0081	0.0008
360	113.4722	0.0098	0.0020
361	113.5312	0.0064	0.0005
362	113.5956	0.0085	0.0005
363	113.6552	0.0058	0.0005
367	113.9015	0.0027	0.0035
368	113.9701	0.0089	0.0005
369	114.0324	0.0089	0.0005
370	114.0935	0.0077	0.0004
371	114.1530	0.0049	0.0004
373	114.2806	0.0078	0.0009
374	114.3419	0.0068	0.0003
*BJD-2455600			

Table 5. (Continued.)

E	The timings of maximum*	$O - C$	error
375	114.4033	0.0058	0.0003
376	114.4689	0.0091	0.0006
377	114.5306	0.0084	0.0004
378	114.5926	0.0081	0.0004
379	114.6569	0.0100	0.0004
380	114.7153	0.0061	0.0006
381	114.7800	0.0085	0.0003
382	114.8435	0.0096	0.0002
384	114.9694	0.0109	0.0007
385	115.0326	0.0117	0.0007
386	115.0927	0.0095	0.0003
387	115.1559	0.0103	0.0010
388	115.2147	0.0068	0.0006
389	115.2835	0.0132	0.0008
390	115.3399	0.0073	0.0010
392	115.4709	0.0136	0.0010
393	115.5332	0.0136	0.0018
392	115.4717	0.0144	0.0006
395	115.6529	0.0086	0.0011
396	115.7114	0.0048	0.0016
397	115.7713	0.0023	0.0007
398	115.8365	0.0052	0.0004
399	115.9003	0.0066	0.0005
402	116.0850	0.0043	0.0005
404	116.2054	0.0001	0.0035
405	116.2673	-0.0003	0.0006
406	116.3333	0.0032	0.0007
407	116.4015	0.0091	0.0004
408	116.4596	0.0049	0.0007
409	116.5183	0.0013	0.0006
410	116.5866	0.0072	0.0008
411	116.6450	0.0033	0.0006
412	116.7064	0.0023	0.0007
413	116.7785	0.0120	0.0007
414	116.8341	0.0054	0.0006
415	116.9003	0.0092	0.0004
419	117.1423	0.0019	0.0006
420	117.2070	0.0042	0.0005
421	117.2664	0.0012	0.0009
422	117.3272	-0.0003	0.0017
423	117.3932	0.0034	0.0006
425	117.5156	0.0011	0.0029
426	117.5742	-0.0027	0.0005
427	117.6438	0.0046	0.0008
428	117.6991	-0.0024	0.0004
429	117.7643	0.0004	0.0005
428	117.6994	-0.0021	0.0003
431	117.9065	0.0179	0.0012
433	118.0121	-0.0011	0.0038
434	118.0766	0.0010	0.0009
435	118.1405	0.0026	0.0004
436	118.1950	-0.0052	0.0007
438	118.3208	-0.0042	0.0003
439	118.3887	0.0014	0.0004
442	118.5750	0.0007	0.0009
*BJD-2455600			

Table 5. (Continued.)

E	The timings of maximum*	$O - C$	error
443	118.6307	-0.0059	0.0006
444	118.6970	-0.0020	0.0005
445	118.7583	-0.0030	0.0005
446	118.8207	-0.0029	0.0007
447	118.8825	-0.0035	0.0005
448	118.9472	-0.0011	0.0009
449	119.0081	-0.0026	0.0006
450	119.0679	-0.0051	0.0007
454	119.3141	-0.0083	0.0020
455	119.3818	-0.0029	0.0009
456	119.4451	-0.0019	0.0021
459	119.6273	-0.0068	0.0012
469	120.2506	-0.0069	0.0004
470	120.3179	-0.0019	0.0016
471	120.3768	-0.0054	0.0014
472	120.4399	-0.0046	0.0004
475	120.6285	-0.0030	0.0007
476	120.6791	-0.0147	0.0006
477	120.7492	-0.0070	0.0003
478	120.8101	-0.0084	0.0007
479	120.8775	-0.0033	0.0006
480	120.9259	-0.0173	0.0007
487	121.3760	-0.0035	0.0014
489	121.4915	-0.0127	0.0010
492	121.6760	-0.0153	0.0002
493	121.7374	-0.0162	0.0015
494	121.7993	-0.0167	0.0004
*BJD-2455600.			

Table 6. Log of the maximum timings of negative superhumps during supercycle 2011 S2

E	The timings of maximum*	$O - C$	error
0	142.3454	-0.0006	0.0005
1	142.4068	-0.0016	0.0004
2	142.4684	-0.0023	0.0009
3	142.5290	-0.0040	0.0007
10	142.9677	-0.0017	0.0012
11	143.0307	-0.0011	0.0011
13	143.1522	-0.0042	0.0019
14	143.2161	-0.0026	0.0010
15	143.2793	-0.0018	0.0014
16	143.3413	-0.0021	0.0008
17	143.4055	-0.0002	0.0006
18	143.4689	0.0008	0.0006
19	143.5318	0.0014	0.0004
20	143.5954	0.0026	0.0008
21	143.6527	-0.0024	0.0005
23	143.7788	-0.0010	0.0005
24	143.8478	0.0056	0.0006
27	144.0266	-0.0026	0.0014
28	144.0810	-0.0105	0.0013
29	144.1471	-0.0068	0.0020
30	144.2141	-0.0020	0.0006
31	144.2813	0.0028	0.0008
32	144.3421	0.0012	0.0006
33	144.4076	0.0044	0.0005
34	144.4658	0.0003	0.0026
35	144.5267	-0.0011	0.0003
36	144.5886	-0.0016	0.0005
37	144.6576	0.0051	0.0005
38	144.7142	-0.0007	0.0013
39	144.7790	0.0018	0.0007
40	144.8413	0.0017	0.0004
42	144.9687	0.0044	0.0013
43	145.0284	0.0018	0.0009
44	145.0887	-0.0002	0.0008
45	145.1539	0.0026	0.0007
46	145.2155	0.0019	0.0007
47	145.2783	0.0023	0.0013
48	145.3405	0.0022	0.0009
49	145.3999	-0.0007	0.0008
50	145.4638	0.0009	0.0011
51	145.5249	-0.0004	0.0010
53	145.6530	0.0030	0.0008
54	145.7172	0.0049	0.0006
55	145.7802	0.0055	0.0009
56	145.8386	0.0016	0.0008
57	145.9026	0.0033	0.0003
61	146.1581	0.0094	0.0012
62	146.2145	0.0035	0.0006
63	146.2764	0.0031	0.0005
64	146.3406	0.0049	0.0008
65	146.3995	0.0015	0.0006
66	146.4646	0.0043	0.0008
67	146.5278	0.0051	0.0005
68	146.5906	0.0056	0.0018
70	146.7147	0.0049	0.0007
*BJD-2455600			

Table 6. (Continued.)

E	The timings of maximum*	$O - C$	error
72	146.8375	0.0031	0.0003
73	146.9020	0.0052	0.0011
74	146.9617	0.0026	0.0004
75	147.0288	0.0073	0.0003
76	147.0829	-0.0009	0.0008
77	147.1530	0.0069	0.0004
78	147.2076	-0.0008	0.0007
79	147.2728	0.0020	0.0004
80	147.3350	0.0019	0.0005
81	147.3984	0.0029	0.0006
82	147.4574	-0.0004	0.0003
85	147.6501	0.0052	0.0006
86	147.7097	0.0025	0.0018
87	147.7691	-0.0004	0.0002
88	147.8363	0.0045	0.0005
91	148.0200	0.0012	0.0006
92	148.0854	0.0042	0.0006
93	148.1477	0.0042	0.0005
94	148.2075	0.0017	0.0004
95	148.2732	0.0050	0.0004
96	148.3331	0.0026	0.0006
97	148.3977	0.0048	0.0003
98	148.4612	0.0060	0.0005
101	148.6461	0.0039	0.0004
102	148.7110	0.0064	0.0005
104	148.8320	0.0027	0.0006
105	148.8975	0.0059	0.0004
106	148.9561	0.0022	0.0007
107	149.0177	0.0014	0.0016
108	149.0844	0.0057	0.0004
109	149.1472	0.0062	0.0003
110	149.2085	0.0052	0.0004
111	149.2722	0.0065	0.0007
112	149.3324	0.0045	0.0004
113	149.3925	0.0022	0.0013
114	149.4613	0.0086	0.0003
115	149.5181	0.0031	0.0009
116	149.5819	0.0046	0.0003
117	149.6458	0.0061	0.0005
118	149.7082	0.0062	0.0010
127	150.2692	0.0061	0.0008
128	150.3324	0.0070	0.0006
129	150.3943	0.0066	0.0013
130	150.4555	0.0055	0.0005
131	150.5220	0.0096	0.0003
132	150.5809	0.0062	0.0005
133	150.6438	0.0067	0.0005
134	150.7072	0.0077	0.0006
135	150.7699	0.0081	0.0004
138	150.9554	0.0066	0.0004
139	151.0228	0.0117	0.0006
140	151.0786	0.0051	0.0005
141	151.1473	0.0115	0.0008
142	151.2041	0.0060	0.0007
143	151.2635	0.0031	0.0006

*BJD-2455600

Table 6. (Continued.)

E	The timings of maximum*	$O - C$	error
145	151.3880	0.0028	0.0018
146	151.4540	0.0065	0.0006
147	151.5133	0.0035	0.0009
148	151.5875	0.0153	0.0007
155	152.0135	0.0049	0.0004
156	152.0766	0.0057	0.0005
157	152.1396	0.0064	0.0006
158	152.2037	0.0081	0.0005
159	152.2618	0.0039	0.0011
160	152.3226	0.0024	0.0014
161	152.3915	0.0089	0.0005
162	152.4547	0.0097	0.0011
163	152.5160	0.0087	0.0005
164	152.5755	0.0059	0.0005
165	152.6365	0.0045	0.0006
166	152.6987	0.0045	0.0003
167	152.7658	0.0092	0.0005
168	152.8256	0.0067	0.0006
169	152.8937	0.0124	0.0007
170	152.9515	0.0079	0.0006
171	153.0137	0.0077	0.0015
172	153.0902	0.0219	0.0021
174	153.2061	0.0131	0.0010
176	153.3277	0.0100	0.0009
177	153.3902	0.0102	0.0011
178	153.4479	0.0055	0.0006
181	153.6401	0.0108	0.0006
182	153.7014	0.0097	0.0008
183	153.7580	0.0039	0.0004
184	153.8180	0.0016	0.0003
185	153.8802	0.0015	0.0004
187	154.0084	0.0050	0.0012
194	154.4416	0.0018	0.0021
195	154.5049	0.0028	0.0005
196	154.5699	0.0055	0.0006
197	154.6327	0.0059	0.0007
198	154.6929	0.0037	0.0009
202	154.9366	-0.0018	0.0023
203	155.0050	0.0042	0.0005
204	155.0681	0.0050	0.0007
205	155.1314	0.0059	0.0003
206	155.1909	0.0030	0.0004
207	155.2549	0.0048	0.0004
208	155.3143	0.0018	0.0006
209	155.3789	0.0041	0.0006
210	155.4403	0.0031	0.0006
211	155.5043	0.0047	0.0004
212	155.5666	0.0048	0.0009
213	155.6312	0.0070	0.0005
219	156.0015	0.0032	0.0005
220	156.0659	0.0053	0.0005
221	156.1251	0.0022	0.0005
222	156.1906	0.0054	0.0006
223	156.2491	0.0015	0.0005
227	156.5012	0.0043	0.0014
*BJD-2455600			

Table 6. (Continued.)

E	The timings of maximum*	$O - C$	error
228	156.5634	0.0041	0.0003
235	156.9970	0.0013	0.0005
236	157.0610	0.0030	0.0007
237	157.1234	0.0031	0.0002
238	157.1854	0.0028	0.0003
239	157.2550	0.0099	0.0207
240	157.3143	0.0069	0.0007
241	157.3705	0.0008	0.0004
242	157.4323	0.0003	0.0004
243	157.4955	0.0011	0.0006
244	157.5601	0.0034	0.0009
245	157.6205	0.0014	0.0009
252	158.0606	0.0052	0.0006
253	158.1237	0.0060	0.0007
254	158.1770	-0.0031	0.0008
259	158.4893	-0.0025	0.0009
260	158.5545	0.0004	0.0010
261	158.6128	-0.0037	0.0005
262	158.6776	-0.0013	0.0005
268	159.0541	0.0013	0.0004
269	159.1116	-0.0036	0.0009
288	160.2913	-0.0084	0.0005
289	160.3576	-0.0043	0.0006
291	160.4815	-0.0051	0.0003
292	160.5446	-0.0044	0.0006
293	160.6096	-0.0018	0.0005
305	161.3556	-0.0038	0.0035
306	161.4259	0.0041	0.0022
307	161.4726	-0.0115	0.0011
308	161.5416	-0.0048	0.0013
309	161.5983	-0.0105	0.0010
317	162.1020	-0.0055	0.0011
318	162.1712	0.0014	0.0020
319	162.2307	-0.0015	0.0050
321	162.3518	-0.0050	0.0013
322	162.4054	-0.0137	0.0014
324	162.5348	-0.0090	0.0008
325	162.5992	-0.0070	0.0006
331	162.9636	-0.0166	0.0028
332	163.0307	-0.0118	0.0015
333	163.0867	-0.0182	0.0012
334	163.1572	-0.0100	0.0018
347	163.9683	-0.0093	0.0008
348	164.0291	-0.0109	0.0005
349	164.0899	-0.0124	0.0009
350	164.1563	-0.0083	0.0006
351	164.2141	-0.0128	0.0006
352	164.2787	-0.0107	0.0011
353	164.3354	-0.0163	0.0021
354	164.4021	-0.0119	0.0008
355	164.4618	-0.0145	0.0017
356	164.5239	-0.0148	0.0016
357	164.5894	-0.0116	0.0008
364	165.0257	-0.0117	0.0073
366	165.1510	-0.0111	0.0005

*BJD-2455600

Table 6. (Continued.)

E	The timings of maximum*	$O - C$	error
367	165.2098	-0.0146	0.0004
368	165.2776	-0.0091	0.0015
369	165.3414	-0.0077	0.0005
370	165.4011	-0.0104	0.0005
415	168.1891	-0.0275	0.0009
416	168.2492	-0.0298	0.0007
417	168.3176	-0.0238	0.0017
418	168.3796	-0.0241	0.0020
419	168.4389	-0.0271	0.0007
420	168.5040	-0.0244	0.0008
421	168.5636	-0.0271	0.0006
435	169.4300	-0.0334	0.0028
436	169.4970	-0.0288	0.0017
437	169.5568	-0.0313	0.0014
451	170.4902	-0.0330	0.0014
452	170.5532	-0.0323	0.0010
460	170.9884	-0.0335	0.0014
463	171.1720	-0.0370	0.0016
466	171.3632	-0.0328	0.0009
467	171.4263	-0.0318	0.0014
468	171.4883	-0.0324	0.0010
469	171.5508	-0.0322	0.0015

*BJD-2455600.

Table 7. Log of the maximum timings of negative superhumps during supercycle 2011 S3

E	The timings of maximum*	$O - C$	error
0	191.4019	-0.0031	0.0007
1	191.4632	-0.0041	0.0008
2	191.5268	-0.0028	0.0010
14	192.2708	-0.0065	0.0049
15	192.3389	-0.0007	0.0006
16	192.4021	0.0003	0.0008
17	192.4646	0.0004	0.0006
31	193.3354	-0.0010	0.0004
32	193.4005	0.0017	0.0005
33	193.4640	0.0030	0.0009
34	193.5271	0.0037	0.0018
48	194.4007	0.0051	0.0012
49	194.4621	0.0042	0.0008
50	194.5210	0.0008	0.0009
51	194.5859	0.0033	0.0006
57	194.9616	0.0052	0.0008
58	195.0240	0.0053	0.0014
59	195.0906	0.0096	0.0010
73	195.9585	0.0052	0.0010
74	196.0199	0.0044	0.0008
76	196.1391	-0.0011	0.0007
95	197.3279	0.0039	0.0007
96	197.3918	0.0055	0.0008
97	197.4532	0.0046	0.0018
111	198.3312	0.0104	0.0008
112	198.3932	0.0100	0.0011
123	199.0810	0.0124	0.0015
124	199.1380	0.0072	0.0008
127	199.3259	0.0081	0.0010
128	199.3872	0.0072	0.0016
138	200.0147	0.0116	0.0021
139	200.0641	-0.0013	0.0011
140	200.1353	0.0076	0.0012
143	200.3277	0.0131	0.0009
144	200.3891	0.0122	0.0006
145	200.4427	0.0034	0.0016
146	200.5142	0.0127	0.0007
154	201.0088	0.0088	0.0011
155	201.0771	0.0148	0.0017
156	201.1347	0.0102	0.0007
159	201.3233	0.0118	0.0009
160	201.3796	0.0058	0.0012
170	202.0009	0.0040	0.0011
171	202.0703	0.0111	0.0013
172	202.1287	0.0073	0.0004
177	202.4423	0.0093	0.0010
178	202.5016	0.0064	0.0006
179	202.5650	0.0074	0.0006
193	203.4386	0.0088	0.0005
209	204.4303	0.0036	0.0021
210	204.4949	0.0059	0.0008
223	205.3069	0.0079	0.0008
224	205.3685	0.0072	0.0010
225	205.4389	0.0153	0.0015
234	205.9934	0.0090	0.0011
*BJD-2455600			

Table 7. (Continued.)

E	The timings of maximum*	$O - C$	error
235	206.0528	0.0061	0.0013
239	206.3033	0.0074	0.0021
240	206.3672	0.0090	0.0008
255	207.2995	0.0067	0.0015
256	207.3633	0.0083	0.0011
257	207.4256	0.0083	0.0005
258	207.4865	0.0068	0.0009
271	208.2957	0.0060	0.0017
272	208.3603	0.0084	0.0016
288	209.3500	0.0011	0.0010
321	211.3999	-0.0050	0.0006
322	211.4662	-0.0010	0.0007
323	211.5279	-0.0016	0.0015
337	212.4022	0.0004	0.0008
338	212.4617	-0.0024	0.0005
367	214.2770	0.0061	0.0039
368	214.3247	-0.0085	0.0012
369	214.3983	0.0027	0.0014
370	214.4530	-0.0049	0.0008
371	214.5138	-0.0063	0.0011
380	215.0692	-0.0117	0.0011
411	216.9987	-0.0136	0.0014
428	218.0501	-0.0214	0.0019
433	218.3678	-0.0153	0.0017
464	220.2951	-0.0194	0.0027
480	221.3068	-0.0046	0.0014
497	222.3590	-0.0116	0.0019
*BJD-2455600.			

Table 8. Log of the maximum timings of negative superhumps during 2012 S1

E	The timings of maximum*	$O - C$	error
0	0.6919	0.0119	0.0008
1	0.7502	0.0080	0.0009
16	1.6849	0.0092	0.0009
17	1.7517	0.0138	0.0004
31	2.6249	0.0158	0.0010
32	2.6840	0.0126	0.0006
33	2.7472	0.0136	0.0010
72	5.1751	0.0145	0.0016
73	5.2297	0.0069	0.0006
74	5.2975	0.0125	0.0006
89	6.2314	0.0129	0.0006
106	7.2932	0.0168	0.0008
107	7.3574	0.0188	0.0005
159	10.5994	0.0248	0.0009
160	10.6621	0.0253	0.0007
161	10.7249	0.0259	0.0008
162	10.7794	0.0182	0.0024
185	12.2157	0.0231	0.0004
187	12.3359	0.0189	0.0004
201	13.2023	0.0140	0.0005
202	13.2718	0.0214	0.0010
224	14.6377	0.0182	0.0013
225	14.7083	0.0265	0.0006
226	14.7560	0.0121	0.0006
240	15.6290	0.0138	0.0008
241	15.6958	0.0184	0.0007
242	15.7551	0.0155	0.0008
256	16.6266	0.0158	0.0005
257	16.6822	0.0091	0.0013
258	16.7496	0.0143	0.0007
271	17.5624	0.0181	0.0010
273	17.6876	0.0188	0.0006
274	17.7460	0.0150	0.0007
287	18.5538	0.0138	0.0014
288	18.6211	0.0188	0.0026
289	18.6748	0.0103	0.0007
290	18.7524	0.0257	0.0010
306	19.7387	0.0164	0.0007
313	20.1770	0.0190	0.0007
314	20.2409	0.0206	0.0004
330	21.2310	0.0151	0.0005
331	21.2906	0.0125	0.0005
335	21.5473	0.0203	0.0012
336	21.6015	0.0122	0.0008
337	21.6687	0.0172	0.0003
338	21.7274	0.0137	0.0007
347	22.2821	0.0082	0.0004
348	22.3473	0.0113	0.0003
352	22.5939	0.0089	0.0012
353	22.6537	0.0065	0.0007
354	22.7152	0.0058	0.0008
368	23.5880	0.0074	0.0019
369	23.6587	0.0158	0.0008
370	23.7115	0.0064	0.0008
382	24.4623	0.0104	0.0020
*BJD-2455900			

Table 8. (Continued.)

E	The timings of maximum*	$O - C$	error
383	24.5219	0.0078	0.0054
402	25.7031	0.0067	0.0005
403	25.7624	0.0037	0.0006
*BJD-2455900.			

Table 9. Log of the maximum timings of negative superhumps during supercycle S2

E	The timings of maximum*	$O - C$	error
0	43.5569	-0.0071	0.0004
1	43.6257	-0.0007	0.0007
2	43.6850	-0.0037	0.0003
3	43.7526	0.0015	0.0004
8	44.0618	-0.0010	0.0008
9	44.1197	-0.0055	0.0004
10	44.1835	-0.0041	0.0008
11	44.2654	0.0154	0.0017
12	44.3027	-0.0096	0.0006
17	44.6160	-0.0081	0.0006
18	44.6802	-0.0063	0.0005
19	44.7437	-0.0051	0.0003
20	44.8049	-0.0064	0.0003
21	44.8697	-0.0039	0.0003
22	44.9345	-0.0015	0.0003
24	45.0607	0.0000	0.0008
35	45.7450	-0.0016	0.0010
36	45.8011	-0.0079	0.0007
37	45.8693	-0.0021	0.0012
38	45.9286	-0.0052	0.0011
39	45.9926	-0.0035	0.0006
45	46.3727	0.0024	0.0011
46	46.4400	0.0074	0.0009
47	46.4986	0.0036	0.0005
50	46.6838	0.0017	0.0007
52	46.8100	0.0032	0.0004
53	46.8625	-0.0067	0.0010
54	46.9418	0.0102	0.0011
55	46.9935	-0.0004	0.0006
67	47.7472	0.0049	0.0007
68	47.8111	0.0065	0.0004
69	47.8683	0.0013	0.0003
70	47.9341	0.0048	0.0005
71	47.9953	0.0036	0.0011
82	48.6836	0.0059	0.0006
83	48.7411	0.0010	0.0005
114	50.6774	0.0041	0.0008
115	50.7451	0.0095	0.0020
137	52.1184	0.0108	0.0006
138	52.1761	0.0061	0.0005
146	52.6694	0.0006	0.0031
147	52.7411	0.0099	0.0002
149	52.8667	0.0107	0.0005
150	52.9204	0.0021	0.0043
154	53.1815	0.0138	0.0004
155	53.2298	-0.0003	0.0007
166	53.9270	0.0109	0.0006
167	53.9913	0.0129	0.0004
173	54.3571	0.0045	0.0009
174	54.4239	0.0089	0.0030
175	54.4871	0.0097	0.0006
177	54.6118	0.0098	0.0004
178	54.6730	0.0086	0.0005
187	55.2342	0.0085	0.0005
188	55.2925	0.0045	0.0004
*BJD-2455900			

Table 9. (Continued.)

E	The timings of maximum*	$O - C$	error
189	55.3591	0.0087	0.0009
190	55.4233	0.0105	0.0006
191	55.4885	0.0133	0.0008
192	55.5500	0.0125	0.0008
193	55.6116	0.0118	0.0011
195	55.7398	0.0152	0.0005
196	55.7995	0.0126	0.0004
197	55.8576	0.0083	0.0009
198	55.9147	0.0030	0.0004
199	55.9842	0.0102	0.0006
200	56.0465	0.0101	0.0005
210	56.6596	-0.0004	0.0007
211	56.7285	0.0061	0.0002
212	56.7908	0.0061	0.0014
213	56.8518	0.0047	0.0011
218	57.1558	-0.0031	0.0010
219	57.2291	0.0078	0.0006
220	57.2899	0.0062	0.0011
221	57.3534	0.0074	0.0006
223	57.4749	0.0041	0.0006
224	57.5327	-0.0003	0.0006
226	57.6528	-0.0050	0.0014
228	57.7883	0.0058	0.0009
229	57.8492	0.0043	0.0004
230	57.9130	0.0057	0.0032
231	57.9782	0.0086	0.0004
232	58.0582	0.0263	0.0052
234	58.1693	0.0126	0.0019
235	58.2270	0.0079	0.0007
236	58.2897	0.0083	0.0015
237	58.3511	0.0073	0.0012
238	58.4122	0.0060	0.0006
239	58.4766	0.0081	0.0004
240	58.5414	0.0106	0.0005
241	58.6007	0.0075	0.0007
242	58.6623	0.0067	0.0003
245	58.8461	0.0034	0.0003
246	58.9127	0.0076	0.0004
247	58.9789	0.0115	0.0006
248	59.0372	0.0074	0.0006
250	59.1678	0.0133	0.0011
251	59.2252	0.0084	0.0006
252	59.2854	0.0061	0.0010
254	59.4140	0.0100	0.0005
255	59.4742	0.0079	0.0014
256	59.5408	0.0122	0.0003
257	59.6029	0.0119	0.0009
258	59.6563	0.0029	0.0008
259	59.7312	0.0155	0.0006
260	59.7876	0.0094	0.0008
261	59.8469	0.0064	0.0005
262	59.9110	0.0082	0.0007
263	59.9791	0.0139	0.0005
266	60.1653	0.0130	0.0011
267	60.2244	0.0097	0.0010
*BJD-2455900			

Table 9. (Continued.)

E	The timings of maximum*	$O - C$	error
268	60.2827	0.0057	0.0006
269	60.3517	0.0123	0.0004
272	60.5384	0.0120	0.0007
273	60.5982	0.0093	0.0004
274	60.6600	0.0089	0.0022
275	60.7216	0.0081	0.0007
276	60.7866	0.0107	0.0003
277	60.8515	0.0132	0.0004
279	60.9712	0.0081	0.0003
280	61.0373	0.0119	0.0003
284	61.2839	0.0090	0.0012
300	62.2835	0.0109	0.0012
301	62.3517	0.0167	0.0007
303	62.4682	0.0086	0.0016
304	62.5336	0.0116	0.0016
305	62.5950	0.0106	0.0049
316	63.2821	0.0117	0.0016
317	63.3413	0.0085	0.0007
318	63.4045	0.0094	0.0014
322	63.6525	0.0079	0.0004
323	63.7118	0.0049	0.0011
324	63.7777	0.0084	0.0004
325	63.8424	0.0107	0.0003
326	63.9041	0.0101	0.0003
332	64.2746	0.0064	0.0009
333	64.3369	0.0064	0.0008
334	64.3981	0.0052	0.0029
335	64.4622	0.0069	0.0009
336	64.5293	0.0116	0.0020
337	64.5895	0.0095	0.0015
338	64.6516	0.0092	0.0023
339	64.7115	0.0068	0.0025
347	65.2125	0.0089	0.0020
348	65.2719	0.0059	0.0012
349	65.3340	0.0056	0.0015
364	66.2550	-0.0088	0.0107
365	66.3299	0.0038	0.0013
366	66.3956	0.0071	0.0017
367	66.4532	0.0023	0.0080
368	66.5094	-0.0039	0.0051
369	66.5773	0.0017	0.0025
370	66.6383	0.0003	0.0021
371	66.7073	0.0069	0.0002
372	66.7645	0.0018	0.0003
373	66.8297	0.0047	0.0011
380	67.2594	-0.0022	0.0015
381	67.3275	0.0036	0.0014
382	67.3953	0.0090	0.0039
383	67.4477	-0.0010	0.0017
384	67.5073	-0.0037	0.0011
386	67.6395	0.0038	0.0004
387	67.7010	0.0029	0.0015
388	67.7612	0.0007	0.0007
389	67.8260	0.0032	0.0007
396	68.2569	-0.0025	0.0006
*BJD-2455900			

Table 9. (Continued.)

E	The timings of maximum*	$O - C$	error
397	68.3225	0.0008	0.0014
398	68.3934	0.0094	0.0011
399	68.4489	0.0024	0.0009
400	68.5112	0.0024	0.0048
401	68.5756	0.0044	0.0008
402	68.6375	0.0040	0.0011
404	68.7648	0.0065	0.0010
405	68.8215	0.0009	0.0004
411	69.1997	0.0049	0.0013
412	69.2693	0.0121	0.0008
413	69.3251	0.0056	0.0005
428	70.2563	0.0014	0.0018
429	70.3202	0.0029	0.0006
430	70.3757	-0.0039	0.0010
431	70.4457	0.0037	0.0008
444	71.2494	-0.0033	0.0024
445	71.3122	-0.0029	0.0010
446	71.3745	-0.0030	0.0008
450	71.6260	-0.0009	0.0006
451	71.6883	-0.0009	0.0004
453	71.8107	-0.0033	0.0003
460	72.2449	-0.0056	0.0008
483	73.6721	-0.0127	0.0005
484	73.7382	-0.0090	0.0005
485	73.8001	-0.0095	0.0006
486	73.8593	-0.0126	0.0024
487	73.9334	-0.0009	0.0029
488	73.9986	0.0020	0.0011
507	75.1697	-0.0119	0.0016
508	75.2275	-0.0164	0.0008
510	75.3576	-0.0110	0.0013
524	76.2239	-0.0177	0.0009
525	76.2906	-0.0135	0.0009
526	76.3473	-0.0191	0.0015
531	76.6570	-0.0213	0.0009
535	76.9046	-0.0231	0.0028
536	76.9652	-0.0249	0.0005
540	77.2188	-0.0207	0.0007
541	77.2757	-0.0261	0.0010
542	77.3456	-0.0186	0.0014
543	77.3995	-0.0271	0.0012
544	77.4730	-0.0159	0.0026
545	77.5165	-0.0347	0.0049
546	77.5930	-0.0207	0.0013
547	77.6582	-0.0178	0.0008
556	78.2144	-0.0229	0.0012
557	78.2700	-0.0296	0.0029
558	78.3321	-0.0299	0.0023
559	78.4029	-0.0214	0.0016
560	78.4656	-0.0211	0.0006
561	78.5323	-0.0168	0.0011
562	78.5949	-0.0165	0.0013
559	78.4023	-0.0220	0.0026
564	78.7156	-0.0205	0.0006
565	78.7758	-0.0227	0.0004

*BJD-2455900

Table 9. (Continued.)

E	The timings of maximum*	$O - C$	error
566	78.8431	-0.0178	0.0011
567	78.8988	-0.0245	0.0004
568	78.9645	-0.0211	0.0004
576	79.4610	-0.0235	0.0023
580	79.7065	-0.0274	0.0006
582	79.8861	0.0350	0.0004
583	79.9516	0.0318	0.0005
594	80.6291	0.0404	0.0005
598	80.8793	0.0396	0.0006
599	80.9474	0.0338	0.0003
604	81.2031	-0.0275	0.0010
606	81.3254	-0.0300	0.0024
615	81.9015	-0.0151	0.0005
*BJD-2455900.			

Table 10. Log of the maximum timings of negative superhumps during supercycle 2012 S3

E	The timings of maximum*	$O - C$	error
0	97.1285	0.0055	0.0007
1	97.1998	0.0144	0.0011
2	97.2467	-0.0010	0.0010
3	97.3101	0.0001	0.0005
10	97.7459	-0.0005	0.0019
11	97.8009	-0.0078	0.0006
12	97.8725	0.0014	0.0007
13	97.9324	-0.0010	0.0004
16	98.1268	0.0064	0.0016
17	98.1821	-0.0007	0.0004
18	98.2440	-0.0012	0.0006
19	98.3111	0.0036	0.0007
24	98.6186	-0.0006	0.0020
25	98.6764	-0.0051	0.0012
26	98.7449	0.0010	0.0009
29	98.9216	-0.0093	0.0006
32	99.1179	0.0001	0.0019
33	99.1651	-0.0151	0.0014
34	99.2442	0.0016	0.0008
35	99.3059	0.0010	0.0009
36	99.3706	0.0034	0.0011
37	99.4256	-0.0040	0.0046
38	99.4864	-0.0055	0.0014
39	99.5562	0.0020	0.0006
43	99.8123	0.0087	0.0036
44	99.8596	-0.0064	0.0019
45	99.9348	0.0065	0.0016
46	99.9912	0.0005	0.0007
47	100.0521	-0.0009	0.0003
48	100.1164	0.0011	0.0006
49	100.1772	-0.0004	0.0007
50	100.2437	0.0037	0.0010
51	100.3063	0.0040	0.0013
52	100.3700	0.0053	0.0007
53	100.4362	0.0092	0.0007
54	100.4960	0.0066	0.0006
55	100.5549	0.0032	0.0004
64	101.1046	-0.0082	0.0018
65	101.1817	0.0066	0.0004
66	101.2416	0.0042	0.0006
67	101.3031	0.0033	0.0007
68	101.3667	0.0046	0.0004
69	101.4326	0.0081	0.0003
70	101.4905	0.0037	0.0018
71	101.5597	0.0105	0.0009
72	101.6111	-0.0004	0.0015
73	101.6778	0.0040	0.0016
74	101.7428	0.0066	0.0003
75	101.7982	-0.0003	0.0004
76	101.8670	0.0061	0.0004
77	101.9293	0.0062	0.0004
82	102.2354	0.0005	0.0045
83	102.3024	0.0052	0.0014
84	102.3614	0.0018	0.0005
85	102.4294	0.0075	0.0012
*BJD-2455900			

Table 10. (Continued.)

E	The timings of maximum*	$O - C$	error
89	102.6644	-0.0069	0.0017
99	103.3034	0.0087	0.0006
100	103.3635	0.0065	0.0004
101	103.4291	0.0098	0.0004
102	103.4956	0.0140	0.0012
103	103.5533	0.0093	0.0005
108	103.8699	0.0141	0.0015
114	104.2434	0.0137	0.0012
115	104.3011	0.0090	0.0005
116	104.3630	0.0085	0.0004
119	104.5510	0.0095	0.0007
120	104.6134	0.0096	0.0009
131	105.2997	0.0102	0.0008
132	105.3628	0.0109	0.0008
133	105.4323	0.0181	0.0006
134	105.4900	0.0135	0.0006
135	105.5506	0.0117	0.0008
136	105.6130	0.0118	0.0006
146	106.2346	0.0099	0.0025
147	106.3052	0.0182	0.0018
148	106.3596	0.0103	0.0007
149	106.4261	0.0145	0.0005
150	106.4897	0.0157	0.0011
151	106.5463	0.0100	0.0024
152	106.6084	0.0098	0.0024
153	106.6783	0.0173	0.0011
160	107.1090	0.0116	0.0009
161	107.1743	0.0146	0.0005
162	107.2327	0.0106	0.0015
163	107.3011	0.0167	0.0010
164	107.3592	0.0125	0.0003
165	107.4213	0.0122	0.0003
166	107.4855	0.0140	0.0010
167	107.5475	0.0137	0.0008
168	107.6096	0.0135	0.0015
177	108.1671	0.0099	0.0007
178	108.2313	0.0118	0.0005
179	108.2988	0.0169	0.0006
180	108.3652	0.0210	0.0008
181	108.4255	0.0189	0.0023
182	108.4826	0.0137	0.0012
183	108.5420	0.0108	0.0004
184	108.6097	0.0161	0.0022
186	108.7275	0.0092	0.0008
187	108.7995	0.0189	0.0010
188	108.8556	0.0127	0.0006
195	109.2988	0.0195	0.0004
196	109.3589	0.0172	0.0003
197	109.4181	0.0141	0.0003
198	109.4814	0.0151	0.0004
199	109.5440	0.0154	0.0005
200	109.6085	0.0175	0.0004
201	109.6689	0.0155	0.0004
202	109.7318	0.0161	0.0009
203	109.7930	0.0150	0.0004

*BJD-2455900

Table 10. (Continued.)

E	The timings of maximum*	$O - C$	error
204	109.8587	0.0183	0.0006
205	109.9214	0.0188	0.0003
211	110.2958	0.0191	0.0004
212	110.3599	0.0209	0.0006
213	110.4176	0.0162	0.0005
214	110.4795	0.0157	0.0004
215	110.5428	0.0167	0.0008
216	110.6042	0.0158	0.0005
218	110.7313	0.0182	0.0004
219	110.7949	0.0194	0.0004
220	110.8566	0.0188	0.0014
221	110.9198	0.0197	0.0006
227	111.3036	0.0294	0.0010
229	111.4168	0.0179	0.0006
230	111.4847	0.0234	0.0004
231	111.5396	0.0160	0.0005
232	111.6095	0.0236	0.0006
233	111.6696	0.0213	0.0011
234	111.7295	0.0189	0.0004
236	111.8545	0.0193	0.0003
241	112.1665	0.0196	0.0010
245	112.3973	0.0010	0.0010
246	112.4567	-0.0019	0.0025
248	112.6085	0.0252	0.0011
260	113.3509	0.0195	0.0013
261	113.4157	0.0220	0.0009
262	113.4774	0.0214	0.0011
266	113.7323	0.0269	0.0004
268	113.8440	0.0139	0.0011
273	114.1640	0.0222	0.0013
271	114.0452	0.0281	0.0012
273	114.1650	0.0232	0.0009
274	114.2261	0.0219	0.0008
276	114.3546	0.0258	0.0006
277	114.4196	0.0284	0.0005
278	114.4791	0.0255	0.0007
279	114.5433	0.0274	0.0006
280	114.6051	0.0269	0.0008
281	114.6646	0.0240	0.0007
283	114.7911	0.0259	0.0006
284	114.8540	0.0264	0.0004
285	114.9148	0.0249	0.0007
288	115.0969	0.0200	0.0078
289	115.1640	0.0247	0.0006
290	115.2175	0.0159	0.0013
292	115.3449	0.0186	0.0007
293	115.4055	0.0168	0.0023
294	115.4704	0.0195	0.0006
295	115.5328	0.0195	0.0005
298	115.7217	0.0214	0.0012
299	115.7842	0.0215	0.0002
300	115.8486	0.0236	0.0007
301	115.9119	0.0245	0.0004
313	116.6657	0.0303	0.0033
315	116.7813	0.0212	0.0006
*BJD-2455900			

Table 10. (Continued.)

E	The timings of maximum*	$O - C$	error
316	116.8453	0.0229	0.0005
317	116.9064	0.0216	0.0003
347	118.7700	0.0150	0.0004
348	118.8358	0.0185	0.0008
349	118.8991	0.0194	0.0003
351	119.0274	0.0231	0.0008
352	119.0875	0.0208	0.0004
353	119.1507	0.0216	0.0006
354	119.2093	0.0180	0.0016
355	119.2810	0.0273	0.0006
356	119.3369	0.0208	0.0005
357	119.4001	0.0217	0.0006
358	119.4616	0.0209	0.0005
359	119.5241	0.0211	0.0007
361	119.6520	0.0243	0.0018
362	119.7117	0.0216	0.0006
363	119.7752	0.0228	0.0024
367	120.0270	0.0253	0.0007
368	120.0880	0.0238	0.0006
372	120.3375	0.0240	0.0008
375	120.4696	-0.0309	0.0006
383	121.0192	0.0200	0.0023
384	121.0776	0.0160	0.0018
385	121.1486	0.0247	0.0012
387	121.2695	0.0209	0.0010
389	121.3952	0.0219	0.0007
394	121.7065	0.0216	0.0005
396	121.8321	0.0224	0.0005
397	121.9005	0.0285	0.0010
398	121.9615	0.0272	0.0008
399	122.0202	0.0235	0.0016
405	122.3920	0.0213	0.0014
407	122.5128	0.0174	0.0011
410	122.7073	0.0249	0.0010
411	122.7661	0.0214	0.0006
412	122.8336	0.0265	0.0007
416	123.0772	0.0207	0.0009
417	123.1422	0.0234	0.0013
419	123.2640	0.0205	0.0036
421	123.3998	0.0316	0.0019
436	124.3218	0.0186	0.0004
437	124.3862	0.0206	0.0010
448	125.0696	0.0182	0.0006
449	125.1290	0.0154	0.0006
450	125.1960	0.0200	0.0005
453	125.3841	0.0211	0.0005
454	125.4396	0.0142	0.0005
455	125.5072	0.0195	0.0007
456	125.5722	0.0222	0.0007
459	125.7548	0.0178	0.0018
460	125.8178	0.0184	0.0012
461	125.8774	0.0156	0.0004
462	125.9335	0.0095	0.0008
465	126.1205	0.0094	0.0025
466	126.1915	0.0181	0.0014

*BJD-2455900

Table 10. (Continued.)

E	The timings of maximum*	$O - C$	error
469	126.3737	0.0132	0.0009
471	126.4965	0.0113	0.0007
484	127.3128	0.0172	0.0014
485	127.3786	0.0207	0.0016
486	127.4282	0.0079	0.0009
490	127.6825	0.0129	0.0004
491	127.7365	0.0046	0.0010
492	127.8025	0.0082	0.0017
493	127.8728	0.0162	0.0007
500	128.3082	0.0152	0.0008
501	128.3750	0.0197	0.0020
502	128.4253	0.0076	0.0009
503	128.4947	0.0147	0.0006
522	129.6769	0.0124	0.0022
523	129.7289	0.0021	0.0008
528	130.0550	0.0165	0.0012
533	130.3596	0.0094	0.0007
534	130.4178	0.0052	0.0008
535	130.4837	0.0088	0.0006
536	130.5454	0.0082	0.0012
555	131.7311	0.0094	0.0006
556	131.7937	0.0097	0.0005
557	131.8586	0.0122	0.0012
*BJD-2455900.			